Electron Trapping by Polar Molecules in Alkane Liquids: Cluster Chemistry in Dilute Solution

Ilya A. Shkrob* and Myran C. Sauer, Jr.

Chemistry Division, Argonne National Laboratory, 9700 South Cass Avenue, Argonne, Illinois 60439

Received: February 1, 2005; In Final Form: April 20, 2005

Experimental observations are presented on condensed-phase analogues of gas-phase dipole-bound anions and negatively charged clusters of polar molecules. Both monomers and small clusters of such molecules can reversibly trap conduction band electrons in dilute alkane solutions. The dynamics and energetics of this trapping have been studied using pulse radiolysis−transient absorption spectroscopy and time-resolved photoconductivity. Binding energies, thermal detrapping rates, and absorption spectra of excess electrons attached to monomer and multimer solute traps are obtained, and possible structures for these species are discussed. "Dipole coagulation" (stepwise growth of the solute cluster around the cavity electron) predicted by Mozumder in 1972 is observed. The acetonitrile monomer is shown to solvate the electron by its methyl group, just as the alkane solvent does. The electron is dipole-bound to the CN group; the latter points away from the cavity. The resulting negatively charged species has a binding energy of 0.4 eV and absorbs in the infrared. Molecules of straight-chain aliphatic alcohols solvate the excess electron by their OH groups; at equilibrium, the predominant electron trap is a trimer or a tetramer, and the binding energy of this solute trap is ca. 0.8 eV. Trapping by smaller clusters is opposed by the entropy that drives the equilibrium toward the electron in a *solvent* trap. For alcohol monomers, the trapping does not occur; a slow proton-transfer reaction occurs instead. For the acetonitrile monomer, the trapping is favored energetically, but the thermal detachment is rapid (ca. 1 ns). Our study suggests that a composite cluster anion consisting of a few polar molecules imbedded in an alkane "matrix" might be the closest gas-phase analogue to the core of solvated electron in a *neat* polar liquid.

1. Introduction

The way in which the excess electron localizes in a dielectric fluid strongly depends on the nature of the fluid.[1] Henceforward, only liquids constituted of polyatomic molecules that have no electron affinity are considered. In many such liquids, the excess electron occupies a void (the solvation cavity) lined by polar (or polarizable) groups of the solvent molecules; the spreading of the electron density onto the solvent is minor. In water and aliphatic alcohols, the ground-state (s) electron is confined in a small, nearly spherical cavity lined by the solvent hydroxyl groups.[2−4] This structure (e^-_{solv}) is stabilized by Coulomb attraction of the electron to positive charges on hydroxyl protons.[4] The binding energy of the solvated electron in such liquids is 1−2 eV,[2,4] and thermal re-excitation of this electron to the conduction band (CB) does not occur (though such a process may occur for excited-state p electrons).[5] Naturally, nonpolar liquids localize the excess electron differently because permanent dipoles in polar groups are absent. In saturated hydrocarbons, the electrons are trapped in large cavities of ca. 7 Å diameter (the so-called "electron bubbles").[6,7] The electron is stabilized by interaction with polarized C−H and C−C bonds in six to eight methyl groups that form the solvation cavity;[8] additional stabilization is provided by electron exchange[9] and/or sharing of the electron density with the solvent molecules.[10] A similar arrangement exists for the solvated electron in the polar liquid acetonitrile (MeCN).[10−13] Although the dipole moment of acetonitrile is large (3.9−4.1 vs 1.6−1.9 D for alcohols),[12] the positive charge resides on the CN carbon that is not accessible to e^-_{solv}. The CN groups point *away* from the cavity; the latter is lined by methyl groups, as in alkane liquids.[10,13] Because the $(MeCN)_2^-$ anion in neat acetonitrile is 450 meV more stable than e^-_{solv}, there is a rapid equilibrium between these two electron states.[10,11,14] Similar equilibria exist for other liquids where more than one electron state is present at any time. In a typical alkane, the binding energy E_t of the electron is only 180−200 meV, and thermal excitation to the CB readily occurs at room temperature.[6,7] Thus, the electron spends some time in a quasi-free state at the bottom of the CB (for which the drift mobility is as high as 10−100 cm^2/Vs),[6,7,15,16] whereas most of the time it dwells in a trapped state (for which the mobility μ_f is only 10^{-3}−10^{-2} cm^2/Vs).[17] For room-temperature *n*-hexane, the probability of finding the electron in a quasi-free state is low, ca. 3×10^{-3}.[6] For hydrocarbons composed of spherical molecules (e.g., 2,2,4-trimethylpentane (*iso*-octane)), the binding energy is 50−60 meV (vs the thermal energy of 25 meV), [7] and this probability is 2 orders of magnitude greater.[7,15,17] In the two-state model for electron conduction in nonpolar liquids,[6,7,16,17] the apparent drift mobility $\langle\mu\rangle \approx \mu_f\tau_f\langle\tau_t^{-1}\rangle$ of the electron depends on the equilibrium fraction of quasi-free electrons (e^-_{qf}) that is reached in reversible reaction 1

$$e^-_{qf} \rightleftarrows e^-_{solv} \qquad (1)$$

where τ_f is the localization time for e^-_{qf} (ca. 20−30 fs for *n*-hexane)[6] and $\langle\tau_t^{-1}\rangle$ is the mean rate of thermal emission from traps ($\langle\tau_t\rangle \approx 8$−9 ps for *n*-hexane).[6] The contribution from trapped/solvated electrons (e^-_{solv}) to the average mobility is

* To whom correspondence should be addressed. E-mail: shkrob@anl.gov.

10.1021/jp050564v CCC: $30.25
Published on Web 06/03/2005

negligible.[6,17] It is usually assumed that the product $\mu_f\tau_f$ exhibits weak temperature dependence[6,7,15−17] (i.e., the activation energy for $\langle\mu\rangle$ is close to the binding energy E_t of electron traps).

What happens to the excess electron in a dilute solution of polar molecules (e.g., alcohol molecules) in a typical nonpolar solvent (e.g., *n*-hexane)? This question, originally posed by Mozumder,[18] still lacks complete resolution. Because the excess electron is attracted to permanent dipoles in the solute molecules, the replacement of nonpolar *solvent* molecules by these polar molecules in the solvation shell of the cavity electron ("dipole coagulation") is energetically favorable. This trend is countered by entropy preventing the substitution. Over time, an equilibrium is reached, and a new type of (solute-)trapped electron emerges. Hereafter, electron "trapping" or "attachment" refers to the formation of a $\{e^-{:}S_n\}_{solv}$ species in which $n \geq 1$ *solute* molecules (S) are included in the first solvation shell of the cavity electron; the *solvent* molecules are still included in the cavity. No S_n^- anions in which the electron occupies a molecular orbital of the *solute* molecule are involved.

Mozumder's paper[18] outlining this scenario stimulated a brief flurry of experimental activity.[19−27] It was expected that small electron clusters, as opposed to solvated electrons in neat liquids, would be simple to study and to model. (Similar expectations were later nurtured for gas-phase cluster anions.) Electron localization in dilute solutions of water and alcohols in liquid[19−26] and vitreous[27] alkanes was studied using pulse radiolysis−transient absorbance (TA) spectroscopy,[19,20,23,24,27] time-resolved conductivity,[21−25] and optically detected magnetic resonance (ODMR).[26] The results obtained in these studies hinted at a complex picture of electron dynamics, and the interest in mixed solvents quickly waned. Nevertheless, a consensus has been reached as to the mechanism for electron localization in such systems (section 2.1). As shown in the present study, this consensual picture requires revision and clarification. In retrospect, alcohols were an inopportune choice for the initial studies because of their tendency to form strongly bound multimers. Our results and analyses suggest that the interest in mixed solvents was fully justified; such systems do provide a new vista on electron solvation in molecular liquids.

To reduce the length of the article, some figures and the Appendix are placed in the Supporting Information. Figures with the designator "S" (e.g., Figure 1S) are placed therein.

2. Background

2.1. Polar Solute Traps in Alkane Solvents. Studies in the 1970s and 1980s[19−26] showed that in dilute solutions of hydroxylic molecules (such as alcohols and water) in normal and branched alkanes, the electrons attach to preexisting clusters S_n (multimers) of these solute (S) molecules.

$$e_{qf}^- + S_n \rightleftarrows \{e^-{:}S_n\}_{solv} \quad (2)$$

Note that because of the occurrence of reaction 1 this electron-trapping reaction can also be represented by reaction 3

$$e_{solv}^- + S_n \rightleftarrows \{e^-{:}S_n\}_{solv} \quad (3)$$

Individual alcohol and water molecules (the "monomers", $n = 1$) do not trap the excess electrons, and in very dilute (<1−5 mM) alkane solutions, localized electrons still reside in solvent traps. By contrast, alcohol clusters present in more concentrated solutions[19−26] bind the electrons quite strongly. H-bonded dimers and higher multimers of hydroxylic molecules form spontaneously in alkanes by reaction 4

$$S + S_{n-1} \rightleftarrows S_n \quad (4)$$

when the mole fraction χ of the solute exceeds 10^{-3}.[19,21,25,28] Let K_n be the equilibrium constant of reaction 4 for solute concentrations given in mole fraction. For open-chain *n*-mers of normal alcohols, Stokes[28] obtained $K_2 = 11$ (with a standard enthalpy of −21.2 kJ/mol), $K_3 = 122.7$, and $K_{n>3} = 76$ (with a standard heat of −23.5 kJ/mol). Using these equilibrium constants and enthalpies, it is easy to obtain the concentrations of various multimers in solution. (Typical speciation plots are given in Figure 1S in Supporting Information.) Less well known is that *acetonitrile* molecules also form clusters in nonpolar solvents, albeit less efficiently than the hydroxylic molecules,[29,30] as shown by the fact that the heat of dimerization of MeCN in CCl_4 is only −6 kJ/mol.[29] In CCl_4 mixtures with $\chi < 0.05$, there is an equilibrium between the antiparallel $(MeCN)_2$ dimer and the monomer.[30b] For $\chi > 0.2$, multimers in which several MeCN molecules couple in an antiparallel fashion to a central molecule are observed.[29,30e] These are mainly pentamers with a typical size of 11 Å.[30e] For $\chi \cong 0.01-0.1$, both trimers (ca. 9 Å)[30e] and pentamers were observed by NMR.[30d]

For small alcohol multimers, electron trapping in the $\{e^-{:}S_n\}_{solv}$ species is reversible (because thermal emission of electrons into the CB is still possible); for larger clusters, the traps are too deep (>1 eV) to observe this emission within the lifetime of the electron species.[20,21,25] The minimum size *n* of the S_n cluster capable of reversible electron trapping is uncertain. Some authors reached the conclusion that alcohol dimers can trap the electrons.[20,21,26] Others concluded that only tetramers or higher multimers can trap these electrons (reversibly and irreversibly, respectively).[19,25] For $\chi < 5 \times 10^{-2}$, this reversible trapping decreases the apparent electron mobility $\langle\mu\rangle$ (by reducing the equilibrium fraction of e_{qf}^- via reaction 2); however, this trapping has almost no effect on the absorption spectrum of the excess electron.[19,20,23] At higher concentration, the absorption peak of the solvated electron shifts toward the blue, and the TA signal increases several fold.[19,20,23] At the onset of this spectral transformation ($\chi \approx 5 \times 10^{-2}$),[19,23] almost no quasi-free electrons are left in the solution.[20,21] For $\chi > 0.2-0.3$, the TA spectrum resembles that for the electron in neat alcohol:[19,20,23] the substitution of solvent molecules by the solute in the first solvation shell of the cavity electron is complete. The lifetime of this electron species (which is a few microseconds) appears to be limited by proton transfer from the alcohol molecule in the solvation shell, as is also the case in neat alcohols.[23] The resulting $\{e^-{:}S_n\}_{solv}$ species should be at least a tetramer.[19] The same applies to the solvated electron observed in water-saturated alkanes,[20,23] though the corresponding spectrum more closely resembles that of the excess electron in dense water vapor[31] and supercritical water[32] than the hydrated electron in liquid water.[2] For $\chi > 0.1$, there is no evolution of the TA spectra after the 30 ps electron pulse.[19] At lower alcohol concentrations (for χ between 0.05 and 0.1), the main effect of the alcohol addition is a decrease in the decay rate of the TA signal on the subnanosecond time scale, which is the expected result of lowering the electron mobility. It appears that electrons are scavenged by large alcohol clusters very rapidly (<30 ps);[19] the rate constant of electron attachment may be $>10^{12}$ M^{-1} s^{-1}.[25] No further growth of the $\{e^-{:}S_n\}_{solv}$ species by dipole coagulation reaction 5

$$\{e^-{:}S_n\}_{solv} + S_m \rightleftarrows \{e^-{:}S_{n+m}\}_{solv} \quad (5)$$

was observed within the first 500 ps after the formation.[19] In fact, this reaction has not been observed even on a longer time

scale.[20−25] The only observation of a cluster-growth reaction similar to reaction 5 is by Ahmad et al.,[22] who observed, albeit indirectly, slow (ca. 7×10^9 M^{-1} s^{-1}) complexation of methanol with the tentative water tetramer in *iso*-octane.

Recently, it has been demonstrated[33] that the electron in supercritical CO_2 (in which the excess negative charge is trapped as the $C_2O_4^-$ anion) forms dipole-bound complexes with the dimers and *monomers* of the alcohols and acetonitrile. In another publication (see sections 4.1 and 1S in ref 10), we observed that the electron in *n*-hexane can be trapped by a *single* acetonitrile molecule. The electron-binding energy of the resulting $\{e^-$:MeCN$\}_{solv}$ species was estimated to be only 200 meV lower[10] than that of the intrinsic solvent trap.[6,7] Ahmad et al.[22] reported reversible trapping of the electron in *iso*-octane by monomers of two other nonhydroxylic polar solutes, trimethylamine and diethyl ether, though the equilibrium constants for electron attachment were very low (ca. 150 and 3.5 M^{-1}, respectively, vs >400 M^{-1} for acetonitrile).[10] Thus, the electron can be trapped by polar *monomers* in solvents other than alkanes. *Acetonitrile* monomers (as well as some other polar molecules missing OH groups) can trap the electron in the alkanes, but *alcohol* molecules have to form clusters. In the present article, we further explore these patterns.

2.2. Pulse Radiolysis of Alkanes: Some Basics. One of the techniques used to characterize $\{e^-$:$S_n\}_{solv}$ species in this study is nanosecond pulse radiolysis−TA spectroscopy. It is appropriate to make some general remarks concerning the radiolysis of neat alkanes and alkane solutions because such an insight is needed to interpret the results given in section 4.1 correctly.

In neat alkanes such as *n*-hexane, two radiolytic products are observed several nanoseconds after the 20 MeV electron pulse in the spectral region of interest (0.5−1.6 μm): trapped electrons, which absorb in the near- and mid-infrared (IR), and olefin cations, which absorb mainly in the blue and ultraviolet (UV) (the $\pi\pi^*$ band) but also have a spectral extension to the visible (the $\sigma\pi^*$ band).[34−36] This TA signal can be observed most distinctively in CO_2-saturated solution (Figure 2Sa, trace (i) in section 4.1) because the TA signal from trapped electrons is removed rapidly by e_{qf}^- scavenging (see below); the cation signal is enhanced (Figure 2Sb) by the slowing of geminate recombination (the mobility of $CO_2^- \ll \langle\mu\rangle$). The mechanism for the formation of these cations (observed as early as 30 ps after the electron pulse)[36] is still uncertain.[34] Fragmentation of vibrationally excited solvent holes (that is, alkane radical cations) and intraspur reactions of these holes and olefins generated via fragmentation of excited solvent molecules are the two most likely routes.[34,37] For cycloalkanes (whose holes are very mobile because of rapid resonance charge transfer),[34,38] the dimer olefin cation is also observed in the red,[35,38] but this species is not formed in *n*-alkanes.[35] The excited state of *n*-hexane (with a yield of 1.6 molecules/100 eV of absorbed energy)[34,39] is short-lived (ca. 300 ps),[39] and its radical cation rapidly deprotonates (in ca. 2 ns).[40] The resulting alkyl radicals, protonated adducts, and olefins absorb in the UV. For *iso*-octane, the excited state and the hole fragment in <40 ps,[39,41] which is much shorter than the duration of the 4 ns fwhm electron pulse used in this study; trapped-electron absorbance in the infrared is also missing because the binding energy is only 50−60 meV.[7] Recent results from Barbara's group[42] suggest that the TA signal from *photoionized iso*-octane observed on the femtosecond time scale[44] likely originates from an *excitonic* species or a close contact pair with the lifetime of ca. 0.4 ps rather than an isolated trapped electron.

For neat *n*-hexane, the Onsager radius r_c (at which the Coulomb interaction between the geminate partners equals the thermal energy, $k_BT \approx 25$ meV) is ca. 300 Å, whereas the average thermalization path of the electron is ca. 80 Å.[44] Thus, <3% of the electrons escape their geminate partner's Coulomb field (become "free") in isolated pairs (ca. 4 pairs/100 eV).[44] Consequently, the yield of free solvated electrons is low (ca. 0.13/100 eV), and because their molar absorptivity ($\epsilon_{1000} \approx 8300$ M^{-1} cm^{-1})[24,45] is also low, a relatively large dose is needed to observe e_{solv}^- on the nanosecond time scale (to obtain an absorbance $>10^{-3}$). The time scale of geminate recombination is given by the Onsager time $t_c = r_c^2/D_e$, where $D_e = (k_BT/e)\langle\mu\rangle$ is the mean diffusion coefficient of the electron (which is much greater than that of the cation). For *n*-hexane at 23 °C, $\langle\mu\rangle \approx 0.092$ cm^2/Vs and $t_c \approx 3.8$ ns. Under the same conditions, the Debye constant $k_D = 4\pi De_c$ for bimolecular charge neutralization in the bulk is ca. 5.3×10^{13} M^{-1} s^{-1}, and the critical concentration $C_{cr} = (4\pi r_c^3)^{-1}$ [46] of electrons at which $k_DC_{cr}t_c \approx 1$ (i.e., cross and geminate recombination occur on the same time scale) is ca. 5 μM. The observed concentration of (free!) electrons at the end of the electron pulse was ca. 0.6 μM (section 4.1). Because the electron concentration for $t < t_c$ is at least an order of magnitude higher than that of the free electrons, the loss of e_{solv}^- to bulk and intraspur cross recombination during the geminate stage is substantial. This is not the case in the photoconductivity experiments discussed in section 4.2 because the yield of free electrons in these experiments is very low (<10 nM). For *isolated* electron−hole pairs, the yield of free electrons does not depend on electron mobility; this yield is entirely determined by the initial electron distribution around the parent hole.[44] Our conductivity measurements suggest that for dilute solutions of acetonitrile or alcohol in alkanes the free-electron yield indeed does not change because of the occurrence of reactions 2 and 3 (see sections 4.2.1 and 4.2.2, respectively). However, in the dose regime typical of pulse radiolysis−TA studies[19−24] (as opposed to pulse radiolysis−dc conductivity studies),[21−23,25] this is not the case. Because for alcohols the electron attachment reaction (eq 2) occurs with a rate constant $>10^{12}$ M^{-1} s^{-1},[25] electron trapping in 0.1 M ethanol occurs well within the geminate stage. Because the mobility of the resulting $\{e^-$:$S_n\}_{solv}$ species (<10^{-2} cm^2/Vs) is much lower than $\langle\mu\rangle$, both cross and geminate recombination are arrested, and the end-of-the-pulse electron yield increases (contrary to the claims made at the end of ref 20). This effect introduces ambiguity in the estimates for molar absorptivity for the $\{e^-$:$S_n\}_{solv}$ species. For an in-depth discussion of this effect (in a different system), see ref 46.

3. Experimental Section

Materials. *n*-Hexane (99+%, Aldrich) and *iso*-octane (99+%, Baker) were passed through activated silica gel to remove olefin impurity. Biotech-grade acetonitrile (99.93+%) stored under N_2 and highest-grade alcohols (99.9+%) and their deuterated analogues (>98+ atom % D) were obtained from Aldrich and were used without purification, but without exposure to air. The alcohol and acetonitrile solutions were deoxygenated by purging with dry nitrogen or argon. All measurements of the electron mobility and TA were carried out in these N_2- or Ar-saturated solutions. Purging these solution or even moving the liquid between the containers causes substantial loss of the polar solute to the headspace. Gas chromatography was used (samples were taken from the exit of the cell, with no exposure of the sample to a headspace) to determine solute concentrations. This monitoring was absolutely necessary; because of the extreme

volatility of polar molecules in dilute hydrocarbon solutions, reproducible results cannot be obtained otherwise. Previous workers[25] reported similar problems; from our experience, the irreproducibility is always traceable to the solute loss.

Electron Mobility. The conductivity setup was the same as described in our previous publication.[6] Fifteen nanosecond fwhm pulses of 248 nm photons from a KrF excimer laser were used to ionize the solutions via biphotonic excitation. Room-temperature solutions were photolyzed in a cell with a 4 cm optical path. To obtain the temperature dependence, 5 μM anthracene solutions were photolyzed in a 2-cm-path cell (photoionization of the anthracene gives higher electron yield compensating for a shorter path). Both cells have two planar Pt electrodes spaced by 6.5 mm operated at 4 kV. For time-of-flight conductivity experiments, the electrode spacing was reduced to 800 μm, and a 100 μm slit was used to generate the charges near the electrodes. A 1064 nm beam from a Nd:YAG laser passed through the cell in the opposite direction to the 248 nm beam and completely enveloped the 248 nm beam inside the cell. The maximum fluence J of 1064 nm photons through the cell was ca. 1.5 J/cm^2 (9×10^{18} photons/cm^2); the fluence of 248 nm light was <0.1 J/cm^2. The typical (free-)electron concentration in our conductivity experiments was 5−10 nM. The lifetime of the electron (<1 μs) is controlled by an electron-scavenging impurity. Under our excitation conditions, cross recombination of charges in the bulk and their movement toward the electrodes were negligible for $t < 1$ μs. The transient photocurrent signal was amplified and recorded with a time resolution of <2 ns. The delay time t_L of the 1064 nm pulse relative to the 248 nm pulse was 25−800 ns; the time jitter between these two pulses was <3 ns. To determine the conductivity signal $\Delta\kappa(t)$ induced by the 1064 nm laser pulse, this laser was pulsed on and off while the 248 nm laser was pulsed for every shot, and the corresponding signals $\kappa_{on}(t)$ and $\kappa(t)$ were subtracted. If not specified otherwise, the measurements were carried out at 23 °C. The conductivity is given in units of nS/cm ($=10^{-7}$ Ω^{-1} m^{-1}).

Pulse Radiolysis−Transient Absorbance (TA). Room-temperature solutions were radiolyzed using electron pulses from the Argonne LINAC (20 MeV, 4 ns fwhm, 21.5 nC per pulse). The solutions were placed in a 2-cm-optical-path cell with Suprasil windows. The analyzing light from a pulsed Xe arc lamp was coaxial with the electron beam and traveled in the opposite direction. A set of 10 nm fwhm band-pass interference filters (50 nm interval) were used for wavelength (λ) selection between 0.5 and 1.6 μm. A fast Ge detector with flat spectral response was used to detect the TA signal on the nanosecond time scale. Čerenkov light and the radiation-induced TA signal from the cell windows ($<10^{-3}$) were subtracted from the kinetic traces, giving the TA signal $\Delta OD_\lambda(t)$ from the irradiated sample versus the delay time t.

4. Results

4.1. Pulse Radiolysis. A typical TA spectrum observed at the end of a 4-ns-fwhm electron pulse in neat *n*-hexane is shown in Figure 1a, trace i. In the first 200 ns, the electron rapidly decays via a scavenging reaction with an impurity and by homogeneous recombination; only the TA signal from the olefin cation (trace ii in Figure 1a; see section 2.2) persists at longer delay times (Figure 2Sa). The addition of 4−50 mM of MeCN increases the TA signal in the near-infrared ($\lambda \approx 0.8-2$ μm), whereas the relative fraction of the olefin cation at $t \cong 50-100$ ns decreases (Figures 3Sa and 4S). The end-of-pulse spectra obtained for 10−50 mM solutions are very similar (Figure 4Sa).

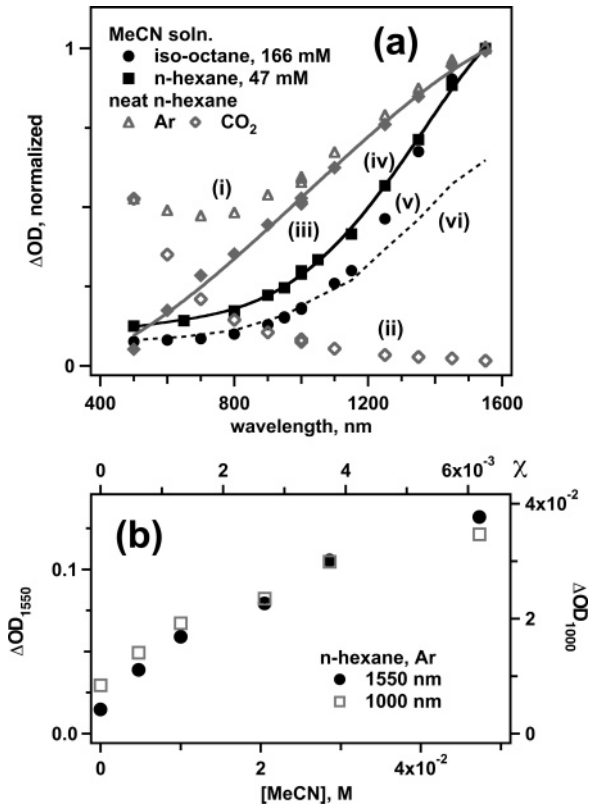

Figure 1. (a) Normalized end-of-pulse TA spectra observed in the pulse radiolysis of Ar-saturated (i) *n*-hexane (open triangles), (iv) 47 mM MeCN in *n*-hexane (filled squares), and (v) 166 mM MeCN in *iso*-octane (filled circles). A 4 ns fwhm, 21.5 nC, 20 MeV electron pulse was used to obtain all of these traces. To facilitate the comparison, the spectra were normalized at 1.55 μm, where only the trapped electron absorbs. Trace ii (open diamonds) shows the spectrum of the solvent olefin cation observed in CO_2-saturated *n*-hexane (see also Figure 2S); this spectrum is normalized at 0.5 μm, where most of the absorbance is from this cation. Trace iii is the difference trace (i.e., electron absorbance). Solid lines are guides for the eye. The dashed line (vi) is scaled-down trace iv drawn to illustrate that TA spectra for $(e^-$:MeCN$)_{solv}$ in the visible are similar for both solvents. (b) End-of-pulse TA signal at $\lambda = 1$ μm (open squares, to the right) and 1.55 μm (filled circles, to the left) vs [MeCN] in Ar-saturated *n*-hexane. The kinetics are shown in Figure 3S.

For $t > 100$ ns, some spectral evolution is observed in the visible (Figure 4Sb) where the olefin cation absorbs. (The dimer anion of acetonitrile may also contribute to this TA signal; see section 1S.) As the trapped electron decays, the relative contribution from the olefin cation increases. The plot of the end-of-pulse TA signal at 1 and 1.55 μm versus [MeCN] is given in Figure 1b; the slight discrepancy between these two plots is due to the interference from the olefin cation that absorbs at 1 μm (Figures 1a and 2Sa). The TA signal first increases linearly with increasing [MeCN] and then "saturates". For *iso*-octane solution, the plot of the 1.55 μm absorbance is linear with [MeCN] to 0.18 M (Figure 5Sa). Otherwise, the spectral evolution is similar to that in acetonitrile/*n*-hexane solutions (cf. Figures 4S and 6S). In both alkane liquids, as the concentration increases, the decay of the TA signal in the infrared becomes slower (Figures 3Sa and 5Sb).

Figure 1a shows a comparison between the electron spectra in neat *n*-hexane, (trace i) and acetonitrile solutions in *n*-hexane and *iso*-octane (traces iv and v, respectively; the spectral profile does not change further at higher concentrations). To facilitate the comparison, all of these spectra are normalized at 1.55 μm. For neat *n*-hexane, the olefin cation signal interferes with the

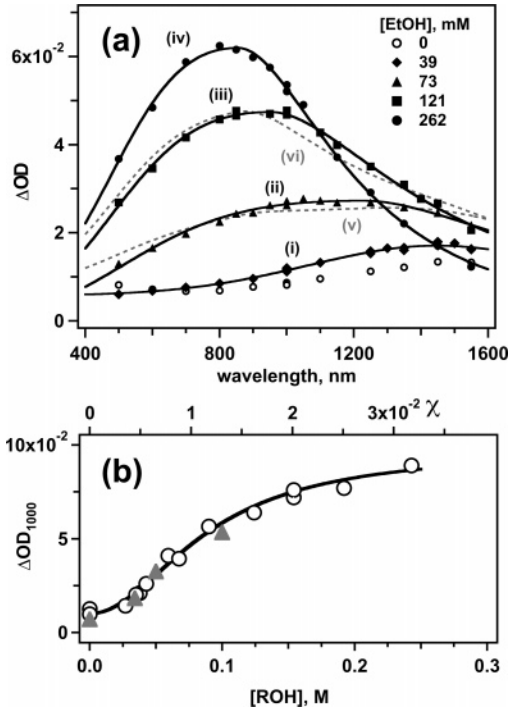

Figure 2. (a) End-of-pulse TA spectra observed in the pulse radiolysis of Ar-saturated *n*-hexane containing 0 mM (open circles), (i) 39 mM (filled diamonds), (ii) 73 mM (filled triangles), (iii) 121 mM (filled squares), and (iv) 262 mM EtOH (filled circles). The solid lines are Lorentzian−Gaussian plots. Dashed lines vi and v are weighted sums of traces iv and i. (b) End-of-pulse 1 μm absorbance vs alcohol concentration for the same system (molar concentration is given at the bottom, mole fraction χ at the top). Open circles are for ethanol, and filled triangles are for 1-propanol (plotted from Figure 4 in ref 23); for the latter solute, the concentrations were scaled down by a factor of 2.

electron signal (see Figure 1a, trace ii), so a direct comparison is difficult. Some compensation can be made by subtracting the spectrum of the olefin cation, trace ii, from the composite spectrum, trace i, assuming that 500 nm absorbance is only from the cation (difference trace iii). Still, it is clear from Figure 1a that the TA spectrum in acetonitrile solution is less broad than that in neat *n*-hexane. The increase in the TA signal from the electron with increasing [MeCN] can be accounted for by the formation of $(e^-{:}\mathrm{MeCN})_{solv}$ species. As shown in section 4.2.1, this trapping becomes nearly irreversible on the observation time scale for [MeCN] > 10 mM. Because it greatly decreases the electron mobility, the efficiency of cross (and, to a lesser degree, geminate) recombination is reduced, which results in a greater electron yield at the end of the 4 ns electron pulse (section 2.2). The magnitude of this effect in our dose regime (ca. 2 times) may be estimated by comparing the yield of the cation absorbance at 500 nm in Ar- and CO_2-saturated *n*-hexane solutions (Figure 2Sb). CO_2 rapidly (<200 ps) scavenges the electron, yielding a slowly migrating CO_2^- anion. The TA signal from the electron at $\lambda = 1$ μm increases ca. 5 times in 50 mM acetonitrile solution. Because there is always a parity between the yields of charges of different sign, it is possible to estimate crudely that the molar absorptivity of the electron at 1 μm is 2−2.5 times greater than that in neat *n*-hexane.

For alcohols (ROH), the spectral evolution is more complex. In Figure 2a, end-of-pulse TA spectra for 40−260 mM ethanol in *n*-hexane are shown. (This system has previously been studied,[20] although the solute concentrations were not reported.) No spectral evolution was observed for $t < 1$ μs for all ethanol concentrations (e.g., Figure 7Sa and 7Sb). Alcohol monomers and multimers are rapidly protonated by the solvent holes, and the formation of olefin cations is thereby suppressed. Consequently, there is no interference from these cations in the TA spectra. However, there is also no spectroscopic evidence for gradual dipole coagulation (reaction 5) on the nanosecond time scale (i.e., all electron equilibria settle in <10 ns (at 23 °C)). The increase of the TA signal at $\lambda = 1$ μm versus [ROH] (Figure 2b) is a sigmoid curve similar to that for acetonitrile except for low alcohol concentrations. This difference is due to the fact that only *multimers* can trap the electron in alcohol solutions (sections 2.1 and 4.2.2), whereas even *single* acetonitrile molecules can trap these electrons (section 4.2.1). A comparison with the TA data in ref 23 (filled triangles in Figure 2b) suggests that the absorbance versus concentration plots for ethanol and 1-propanol are identical when [PrOH] is scaled down by a factor of 2. As shown in section 4.2.2, the plots for $\langle\mu\rangle$ versus [ROH] are also similar for all alcohols studied once their concentrations are appropriately scaled. As [ROH] increases, the decay kinetics (such as those for acetonitrile, Figure 3Sa) observed on the submicrosecond time scale slow (Figure 3Sb). For both solutes, this decrease is significant in dilute solutions (<20−50 mM); at higher concentrations (when the trapping becomes irreversible, see sections 4.2.1 and 4.2.2), further slowing down of these kinetics does not occur. The magnitude of the increase in ΔOD_λ for $\lambda = 1$ μm is ca. 9 times for [EtOH] ≈ 0.26 M (Figure 2b). Because, as noted above, part of this increase (ca. 2 times) is due to the suppression of recombination, the rough estimate for the increase in the $\lambda = 1$ μm absorptivity of the trapped electron is 4−5 times.

The crucial difference between the acetonitrile and ethanol solutions is that for the latter solute not only the amplitude of the TA signal increases as [S] increases but also the spectral profile evolves continuously (Figure 2a). The band maximum shifts from 1.5 μm at 40 mM to 1.1 μm at 73 mM to 0.95−1 μm at 120 mM to 0.8 μm at 262 mM. One can inquire whether the TA spectra observed at the intermediate ethanol concentrations can be obtained by addition of weighted spectra observed at the highest and the lowest ethanol concentrations (dotted lines in Figure 2a). Such would be the case if only one kind of the $(e^-{:}S_n)_{solv}$ species was present in the reaction mixture. Although these weighted sums can be made close to the spectra observed, this does not seem to be the case (Figure 2a). This argues that only a few (perhaps 2 to 3) types of trapped electron species are present in the solution at equilibrium, as previously suggested by Gangwer et al.[25] and others.[20−24] We will return to these observations in section 5.2.

4.2. dc Photoconductivity Studies. *4.2.1. Acetonitrile.* Figure 3a and b shows the typical photoconductivity signals $\kappa(t)$ from the electrons generated by 248 nm photon ionization of dilute acetonitrile solutions in Ar-saturated, room-temperature *n*-hexane. Qualitatively, very similar kinetics were observed using 5 μm anthracene (added to increase the photoionization yield). The conductivity signal ($t < 2$ μs) decays exponentially to a plateau as $\kappa(t) = \kappa_0 \exp(-kt) + \kappa_i$. (This constant offset is subtracted from the traces shown in Figure 3.) The exponential decay is due to the reaction of the electron with an impurity or the polar solute (see below); the plateau conductivity κ_i is from ions that decay slowly (on the millisecond time scale) by recombination in the bulk and neutralization at the electrodes. This residual ion signal does not depend on the acetonitrile concentration (<60 mM), suggesting that the *addition of acetonitrile has no effect on the electron yield.* The conductivity signal κ_0 from (free) electrons can be obtained by exponential extrapolation to zero time; this quantity is plotted versus [MeCN] in Figure 4a (open circles, to the left). Note that for the electron

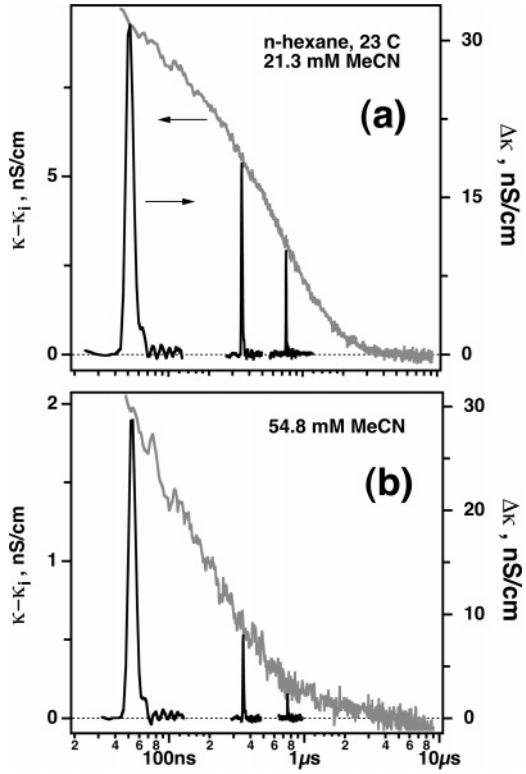

Figure 3. Decay kinetics of dc photoconductivity signal κ from Ar-saturated solutions of *n*-hexane containing (a) 21.3 and (b) 54.8 mM MeCN (to the left). The signal from the ions (κ_i) is subtracted; the residual signal is from the electron. The solution was photoionized using a 15 fwhm pulse of 248 nm light; trapped electrons were subsequently photoexcited using a 6 ns fwhm, 9×10^{18} photons/cm^2 pulse of 1064 nm light. The 1064 nm photon-induced signal ($\Delta\kappa$) plotted to the right has the same temporal profile as the excitation pulse; the decrease in the amplitude as a function of the delay time t_L of the 1064 nm pulse faithfully follows the $\kappa - \kappa_i$ kinetics. See also Figures 9Sa and 16S.

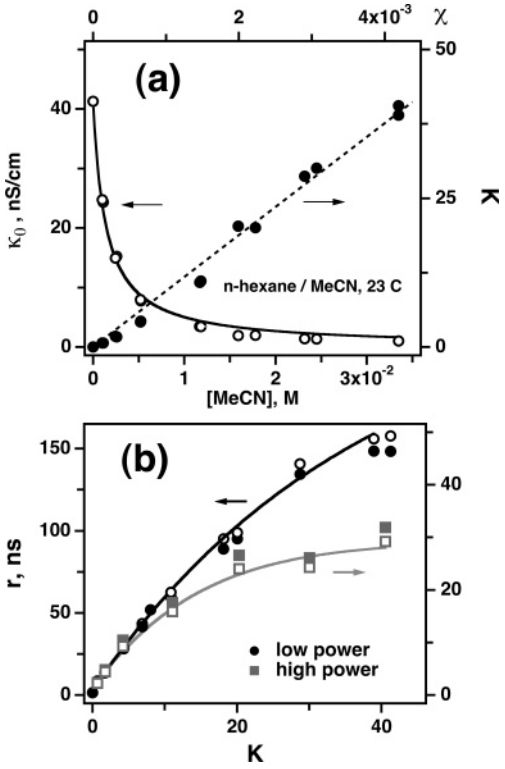

Figure 4. (a) Concentration dependence of the extrapolated electron conductivity κ_0 (open circles) for 248 nm photoexcitation of MeCN in Ar-saturated room-temperature *n*-hexane (to the left). The concentration dependence of parameter $K = \langle\mu_n\rangle/\langle\mu\rangle - 1$ (filled circles, to the right) is shown for the same system. The solid line is calculated using eq 6, and the dashed line is a linear fit; the slope of this line gives the equilibrium constant of reaction 3. (b) Ratio r (for $t_L \approx 50$ ns) for the same system determined using 8.1×10^{18} photon/cm^2 (circles, to the left) and 5.4×10^{17} photon/cm^2 (squares, to the right) pulses of 1064 nm light. See Figure 11S for power dependencies at different MeCN concentrations. Open symbols indicate the numerical integration of $\Delta\kappa$ signals; filled symbols indicate the integrals of least-squares-optimized Gaussian fits. Compare with the r vs K plot for ethanol/*n*-hexane solutions given in Figure 20Sb.

concentrations generated in our conductivity experiments (a few nM) second-order recombination on the nano- and microsecond time scales is very minor.

The addition of acetonitrile creates a new kind of electron trap in a dynamic equilibrium with e^-_{qf}. Following the approach of ref 10 (further developed in the Appendix), we introduce the equilibrium constant K_{eq} of reaction 3 between the electrons in the solvent trap, e^-_{solv}, and in this monomer solute trap, $\{e^-$:MeCN$\}_{solv}$. As the *net* molar concentration c of the solute increases, the equilibrium fraction of e^-_{solv} and the apparent mobility $\langle\mu\rangle$ of the electron decrease as

$$\frac{\langle\mu\rangle}{\langle\mu_n\rangle} = (1 + K_{eq}c)^{-1} \qquad (6)$$

where $\langle\mu_n\rangle$ is the apparent electron mobility in *neat n*-hexane. Provided that the electron yield does not change with the solute concentration (as is the case in acetonitrile solutions, see above), the ratio of the corresponding conductivity signals κ_0 is given by eq 6. The decay rate of the electron decreases in proportion to the mobility $\langle\mu\rangle$ for $c < 0.03$ M, as can be seen from the correlation plot given in Figure 4Sb in ref 10. At higher concentrations, the rate constant k gradually begins to increase, possibly because of dimer formation (section 1S). Equation 6 may be conveniently expressed as $K = K_{eq}c$, where $K = \langle\mu_n\rangle/\langle\mu\rangle - 1$. (The concentration plot for this quantity is given in Figure 4a, with solid circles to the right.) In either form, eq 6 can be used to fit the plot of $\kappa_0 \propto \langle\mu\rangle$ versus [MeCN] both for *n*-hexane and *iso*-octane solutions. The slope of the van't Hoff plot for the resulting constant K_{eq} obtained at different temperatures yields the standard heat $-\Delta H^0_{eq}$ of reaction 3 for the MeCN monomer. In ref 10 (see section 1S in the Supplement and Figure 7b in section 4.2.2 of the present paper), we have carried out just such an analysis and have obtained $K_{eq} \approx 440 \pm 20$ M^{-1} (at 25 °C) and $-\Delta H^0_{eq} \approx 19.6 \pm 0.9$ kJ/mol (ca. 200 meV).[10] For dilute *iso*-octane solutions ([MeCN] < 30 mM), eq 1 also holds (Figure 8Sa), and $K_{eq} \approx 950 \pm 50$ M^{-1} at 25 °C.

Because for *iso*-octane $\langle\mu\rangle$ is 6700 times greater than the combined anion and cation mobility μ_i (ca. 10^{-3} cm^2/Vs)[7b,c] whereas for *n*-hexane $\langle\mu\rangle$ is only ca. 56 times greater than μ_i (ca. 1.5×10^{-3} cm^2/V s),[7c] the former solvent gives a better opportunity to follow the decrease in the electron mobility for $\chi > 5 \times 10^{-3}$ because even at this high solute concentration $\langle\mu\rangle > \mu_i$. (The typical kinetics are shown in Figure 9S.) As shown in Figure 8Sb, where κ_0 is plotted versus [MeCN] on the logarithmic scale, $\langle\mu\rangle$ decreases by a factor of 300 between 32 and 175 mM in the concentration range where eq 6 is no longer applicable. It is precisely this concentration range that was explored in section 4.1. Thus, the equilibrium was completely shifted toward the acetonitrile traps, and the spectra shown in Figure 1 are from such traps. (The same pertains to *n*-hexane solutions.) Given the constancy of the spectrum as a

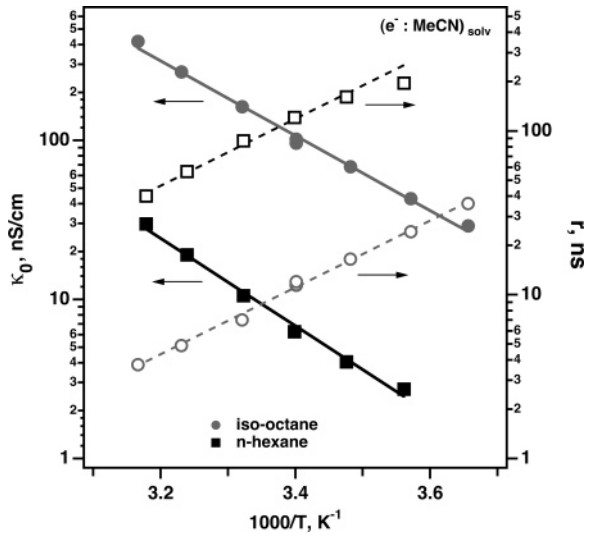

Figure 5. Arrhenius plots for extrapolated conductivity signals κ_0 ($t \rightarrow 0$) from electrons (filled symbols and solid lines, to the left) and ratio r for $t_L = 50$ ns and $J = 9 \times 10^{18}$ photon/cm^2 (open symbols and dashed lines, to the right) in a 17.3 mM solution of MeCN in *n*-hexane (squares) and a 22 mM solution of MeCN in *iso*-octane (circles). The corresponding activation energies for κ_0 and r are 52.7 ± 2.2 and 39 ± 1.8 kJ/mol (*n*-hexane) and 45.1 ± 1.3 and 39 ± 0.9 kJ/mol (*iso*-octane), respectively.

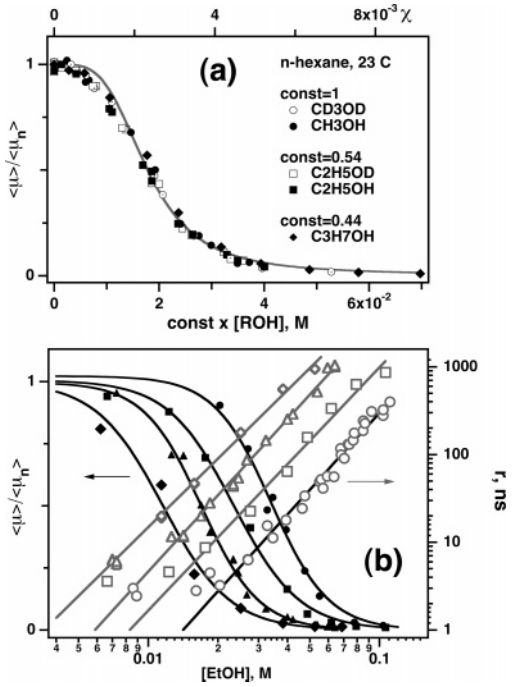

Figure 6. (a) Plot of normalized electron mobility (i.e., normalized κ_0 signal) vs const × [ROH] for solutions of methanol (filled circles), methanol-d_4 (open circles), ethanol (filed squares), ethanol-d_1 (open squares), and 1-propanol (filled diamonds) in Ar-saturated *n*-hexane at 23 °C. The molar concentration is given at the bottom; mole fraction χ is given at the top. The scaling constants are 1, 0.54, and 0.44 for methanol, ethanol, and 1-propanol, respectively. The solid line is a fit to eq 9 with $m \approx 3.5$and $c_0 \approx 18$ mM. Observe the universality of the behavior for all alcohols and their isotopes. (b) To the left: normalized electron mobility (filled symbols) vs net [EtOH] for 1.7 °C (diamonds), 8.1 °C (triangles), 14.9 °C (squares), and 23 °C (circles) plotted on a logarithmic concentration scale. The solid lines are optimum fits obtained using eq 9. To the right: concentration plots for ratio r (open symbols, for the same excitation conditions as in Figure 5); note the logarithmic scale. The same symbol shapes as in plot a are used. The straight lines drawn through the symbols correspond to the exponential power of ca. 2.8.

function of [MeCN], it may be expected that $\{e^-$:MeCN$\}_{solv}$ is the predominant species in both solvents. Thus, it is not presently clear what causes the decrease of $\langle\mu\rangle$ in concentrated acetonitrile/*iso*-octane solutions. The entire plot in Figure 8Sb can be fit using the empirical equation $\langle\mu_n\rangle/\langle\mu\rangle = 1 + K_{eq}c + K_n c^n$, with $n \approx 3.6$. This suggests that a multimer species in equilibrium with $\{e^-$:MeCN$\}_{solv}$ might be involved at high MeCN concentrations (section 1S). The vis-absorbing, covalently bound $(MeCN)_2^-$ anion occurs in neat acetonitrile,[10,11,14] and this species may also occur in the *iso*-octane solutions. Another possible rationale is that at high concentration solute molecules scatter quasi-free electrons, thereby changing $\langle\mu\rangle$. Because our interest is mainly in the cavity electrons, hereafter we focus on *dilute* solutions (<30 mM) for which the multimer anion formation and/or electron scattering may be safely neglected.

For sufficiently concentrated acetonitrile solutions (yet still within the range of applicability of eq 6), $K \gg 1$ and $\log\langle\mu\rangle - \log\langle\mu_n\rangle \propto -\Delta H^0_{eq}$. Thus, the enthalpy $-\Delta H^0_{eq}$ can be estimated as the difference in activation energies E_μ* and $E^*_{\mu n}$ of the electron mobility (and, therefore, κ_0) in the acetonitrile solution and neat solvent, respectively. Figure 5 demonstrates the Arrhenius plots for κ_0 in 17.3 mM MeCN in *n*-hexane (the corresponding kinetics are shown in Figure 10S) and 22 mM MeCN in *iso*-octane.[48] At these concentrations, $\langle\mu\rangle$ decreases >10 times versus the value for neat solvents. The activation energies for *n*-hexane and *iso*-octane are 4.9 ± 0.7 and 32.6 ± 0.4 kJ/mol (for neat solvents) and 52.7 ± 2.2 and 45.1 ± 1.3 kJ/mol (for MeCN solutions), respectively, from which $-\Delta H^0_{eq}$ is estimated to be 20.1 ± 3 and 48 ± 3 kJ/mol, respectively. Note that in neat *n*-hexane the binding energy for the electron trap is ca. 200 meV (i.e., the binding energy of the acetonitrile trap versus the CB edge is ca. 400 meV). A better, more reliable estimate for the same parameter (that does not require making an assumption that the product $\mu_f\tau_f$ is temperature-independent)[6,7] can be obtained using 1064 nm (1.17 eV) photon-induced electron detachment,[6] as described below.

Figure 3 shows the effect of 1064 nm photoexcitation on the conductivity signal from the electron. (See also Figures 9Sa and 10Sb.) The temporal profile of the difference signal $\Delta\kappa$ (section 3) follows the Gaussian profile of the 1064 nm pulse. At all solute concentrations and temperatures, the amplitude of the $\Delta\kappa$ signal decreases with the delay time t_L of the 1064 nm laser pulse in the same way that $\kappa_e(t_L) = \kappa(t_L) - \kappa_i$, the conductivity signal from the electron induced by 248 nm light, decays. When the electrons are scavenged (as $\kappa(t)$ decays to a plateau within 1−5 μs), 1064 nm light does not produce any increase in the conductivity.[49] This behavior suggests that the $\Delta\kappa$ signal originates from 1064 nm photons detaching the electron from the traps and promoting these electrons into the CB of the solvent. The equilibrium is rapidly reestablished, but the conductivity increases significantly during the 1064 nm laser pulse. Observe that all $\Delta\kappa(t)$ kinetics eventually approach zero (i.e., there is no inhibition of geminate recombination due to the photodetrapping). As shown by Lukin et al.,[50] such a process is significant only for $t_L < t_c/10$ (i.e., on the time scale that is much shorter than the duration of the 248 nm pulse).

It has been demonstrated[6] that the ratio r of the area $\Delta A(t_L) = \int dt\, \Delta\kappa(t)$ under the $\Delta\kappa(t)$ kinetics to the electron conductivity $\kappa_e(t_L)$ prior to the photoexcitation is given by

$$r = \frac{\Delta A(t_L)}{\kappa_e(t_L)} \approx \langle\sigma_t\tau_t\rangle J \qquad (7)$$

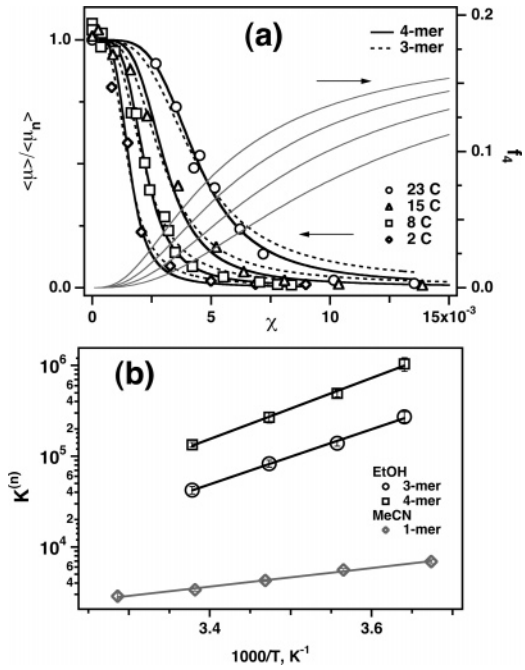

Figure 7. (a) To the left: normalized electron mobility vs nominal c = [EtOH] (the same data and symbol shapes as in Figure 6b). The solid and dashed lines drawn through the symbols are fits obtained using eq 11 for a tetramer and a trimer, respectively. To the right: estimated mole fraction $f_4 = 4[S_4]/c$ of the tetramer at equilibrium vs c for the four temperatures given in Figure 6b; the higher fraction corresponds to the lower temperature. (b) van't Hoff plots for the equilibrium constant of reaction 3 for the tentative trimer (circles) and tetramer (squares) of EtOH and for the MeCN monomer (diamonds). Vertical bars indicate 95% confidence limits of the least-squares fit to eqs 11 and 6 for ethanol and acetonitrile, respectively.

where σ_t is the cross section for electron photodetachment from a given trap, τ_t is the lifetime of the electron in this trap, and $\langle ... \rangle$ stands for the average over all such traps weighted by their equilibrium fractions. As seen from eq 7, this ratio does not depend on the delay time of the 1064 nm pulse (in accordance with Figure 3) and is independent of electron mobilities and yields as well. Equation 7 is valid only for low fluence J of the 1064 nm light (i.e., when the deviation from the equilibrium is relatively small). At high fluence, the equilibrium is shifted during the pulse, and a phenomenon akin to saturation sets in. (See the Appendix for more discussion.) The typical plots of r versus J are shown in Figure 11Sa. In Figure 11Sb, the ratio r is normalized by its value r_{max} attained at the maximum fluence J_{max} of 1064 nm photons (ca. 8.5×10^{18} photons/cm^2). As seen from the latter plot, the ratio r first increases linearly with increasing fluence (for $J < 10^{18}$ photons/cm^2) with a slope that weakly depends on [MeCN] and then saturates (Figure 11S). In Figure 4b, the ratios r are plotted for $J \approx 5.4 \times 10^{17}$ photon/cm^2 (squares) and 8.1×10^{18} photon/cm^2 (circles) as functions of K ($\approx K_{eq}c$). The higher fluence corresponds to the "saturation" regime, whereas the lower fluence corresponds to the linear regime (eq 7). The two curves exhibit the same initial slope but diverge at higher concentrations as the equilibrium shifts toward $\{e^-$:MeCN$\}_{solv}$. Very similar behavior is obtained using the two-trap model in the Appendix. The plateau value ($r \approx 30$ ns) at the lower fluence is attained when reaction 3 is completely shifted toward the right side. Using eq 7, $\sigma_t\tau_t \approx 5.6 \times 10^{-26}$ cm^2 s is obtained for this trap. For electrons in neat *n*-hexane, $\sigma_t\tau_t \approx \sigma_t\tau_t \approx 2.5 \times 10^{-28}$ cm^2 s,[24] (i.e., for electrons in the acetonitrile traps, the product $\sigma_t\tau_t$ is ca. 225 times greater). In section 4.1, we estimated that the absorption cross section at $\lambda = 1$ μm for an electron captured by the acetonitrile trap is ca. 2 times greater than that of e^-_{solv}. Using the estimate of 8.3 ps for τ_t in *n*-hexane[6] and assuming unity quantum yield for electron photodetachment (justified in section 5.2), we estimate that the residence time τ_i for $\{e^-$:MeCN$\}_{solv}$ is ca. 1 ns. In Figure 5, Arrhenius plots of the ratio r (Figures 9Sb and 10Sb for kinetic traces) are shown for the same two concentrations used to estimate $-\Delta H_{eq}$. At these concentrations, the equilibrium is shifted toward $\{e^-$:MeCN$\}_{solv}$ so that the activation energy for this ratio approximately equals that of the detrapping rate. The latter activation energy is commonly identified with the binding energy E_t of the trapped electron with respect to the CB edge.[6,7,16] For *n*-hexane and *iso*-octane, estimates of 39 ± 2 and 39 ± 1 kJ/mol were obtained, respectively. These two estimates agree perfectly with the estimate of $E_t \approx 400$ meV given above. The closeness of binding energies for the two alkanes qualitatively accounts for the similarity of the TA spectra shown in Figure 2.

4.2.2. Alcohols in n-Hexane. Figure 12S shows a family of $\kappa(t)$ kinetics for 248 nm photoexcitation of 12 mM ethanol in *n*-hexane solutions for several temperatures between 2 and 42 °C. As is observed for acetonitrile, these kinetics decay exponentially (except for the lowest temperatures; see below); otherwise, the two systems show quite different behavior.

First, in alcohol solutions the conductivity signal κ_i from the ions depends on [EtOH] (Figure 13S). The concentration dependence of κ_i is the same in solutions with and without anthracene. Other photosensitizers, such as benzene and triethylamine, exhibit the same concentration dependence for κ_i, save for a scaling factor. Moreover, the same κ_i versus [EtOH] plots are observed in SF_6- and CO_2-saturated solutions, where the electrons are promptly converted to anions. Almost the same dependencies are observed at lower temperatures (Figure 13S). Time-of-flight experiments (Figure 14Sa shows a few typical traces) indicate that the addition of ethanol *decreases the mobility of fluoride anions* in SF_6-saturated hexane solution (with 0.65 mM triethylamine added as a photosensitizer). For the cation, no such decrease was observed. The decrease in the anion mobility (ca. 2 times for 0.12 M ethanol, Figure 14Sb) is very substantial, and it readily accounts for the observed decrease in κ_i (Figure 13S), suggesting that the ionization yield *does not* depend on the alcohol concentration, as is also the case for acetonitrile.[51]

Second, for alcohols the electron conductivity κ_0 decreases with increasing [S] in a qualitatively different way than for acetonitrile because it does not follow eq 6. This dependence does not change upon deuteration: it is exactly the same for CH_3OH and CD_3OD and C_2H_5OH and C_2D_5OD (Figure 6a). By appropriately scaling [ROH], the same κ_0 versus [ROH] dependence was observed for methanol, ethanol, and 1-propanol (Figure 6a). Because all of these dependencies are the same, in the following only ethanol solutions are considered; this solute is representative of other *normal* alcohols. Baxendale and Sharpe[21] reported that qualitatively different behaviors were observed for different *n*-alcohols. Our results suggest otherwise. The likely problem with the previous measurement was inadequate control of alcohol concentration (section 3).

For ethanol solution, κ_0 does not decrease until $\chi > 0.01$; at higher concentration, $\langle \mu \rangle$ decreases rapidly, and for $\chi \approx 0.1$, almost no e^-_{qf}'s remain in the solution because of the occurrence of reaction 2. The decay rate of $\kappa(t)$ decreases as $\langle \mu \rangle$ decreases; however, unlike the situation in acetonitrile solutions, the addition of a 1−5 mM alcohol actually *increases* the rate constant $k = k_n + \Delta k$ of the exponential decay (k_n is the constant

observed in neat *n*-hexane) with little change in the apparent electron mobility (Figure 15S). This behavior (for 1-propanol) is in agreement with the pulse radiolysis−TA study by Baxendale and Rasburn.[23] Gangwer et al.[25] reported that the bimolecular rate constant $k_{\mathrm{eff}} \approx \Delta k/c$ for electron scavenging by methanol in *n*-hexane decreases from 4×10^8 M^{-1} s^{-1} (the same limiting rate constant was obtained by Baxendale and Rasburn)[23] at 0.1 mM to 10^8 M^{-1} s^{-1} at 5 mM. Their time-of-flight measurement suggested (in agreement with our results) that $\langle\mu\rangle$ did not change significantly at these low methanol concentrations.[52] As shown in Figure 16Sa and 16Sb, in the course of the scavenging reaction occurring in this low-concentration regime (at 2 °C and 21.5 °C, respectively), the ratio *r* *does not* change with the delay time t_{L}. This argues against the occurrence of slow reaction 3 in these very dilute solutions. (The trapping would increase the retention time of the electron in the trap, thereby increasing ratio *r* at longer delay times t_{L}.) In principle, the initial increase in the decay rate *k* may be explained by a scavenging reaction involving an electron-attaching impurity present in the *solute*, such as an aldehyde.[25] Our control experiments as well as gas chromatography suggest that the aldehyde concentration is too low to account for the observed effect. A crucial observation is that the initial bimolecular rate $k_{\mathrm{eff}} \approx \Delta k/c$ decreases by ca. 20% when deuterated alcohols are used instead of protiated ones, both for ethanol and methanol (Figure 15Sa and b, respectively). Only a proton transfer would exhibit such a considerable isotope effect. (Notice that no isotope effect was observed for electron mobility, Figure 6a.) All of these observations point to a slow ($<5 \times 10^9$ M^{-1} s^{-1} vs a typical electron attachment constant of $(1-3) \times 10^{12}$ M^{-1} s^{-1}),[19,25] inefficient reaction of the trapped electron with the ethanol monomer via a proton-transfer reaction

$$e^-_{\mathrm{solv}} + \mathrm{ROH} \rightleftarrows \{e^-{:}\mathrm{ROH}\}_{\mathrm{solv}} \rightarrow \mathrm{RO}^- + \mathrm{H}^\bullet \qquad (8)$$

(The hydrogen atom subsequently reacts with the solvent). Proton-transfer reaction on the microsecond time scale analogous to eq 8 also occurs[23,53] for solvated electrons in *neat* alcohols, where the cavity electron is stabilized against the proton transfer by strong electrostatic interactions with several OH groups.[54] Such a stabilization mechanism is lacking for $\{e^-{:}\mathrm{ROH}\}_{\mathrm{solv}}$, and after formation, this species either promptly dissociates or undergoes proton transfer. Direct, prompt deprotonation of alcohol monomers in their encounter complex with the solvated electrons was previously postulated by Baxendale and Rasburn;[23] our results further support their suggestion.

At higher alcohol concentrations ($\chi > 0.01$), the electron mobility rapidly decreases with the net solute concentration *c* of the alcohol (Figure 6a and b). Following Baxendale and Sharpe,[21] the decrease in $\langle\mu\rangle$ can be described by the empirical equation

$$\frac{\langle\mu_n\rangle}{\langle\mu\rangle} = 1 + \left(\frac{c}{c_0}\right)^m \qquad (9)$$

that generalizes eq 6, where *m* is the mean number of solute molecules per $\{e^-{:}S_m\}_{\mathrm{solv}}$ cluster and c_0 is a (temperature-dependent) characteristic concentration. The data in Figure 6b can be fit using this equation assuming temperature-independent $m \approx 3.5$ (c_0 is ca. 18 ± 1 mM at 23 °C). Thus, in agreement with Gangwer et al.[25] we conclude, contrary to Baxendale and co-workers,[20−24] that *only higher multimers* trap the electron in alcohol solutions at equilibrium. To make more quantitative estimates, the following model was used.[25] The alcohol molecules were assumed to cluster according to reaction 4 with the equilibrium constants K_n given in section 2.2, and solvated electrons e^-_{solv} were assumed to attach to these multimers via reaction 3 with the equilibrium constants $K^{(n)}_{\mathrm{eq}}$. The tacit assumption of this scheme is that reaction 3 is much faster than reaction 4. From eq 4, we have $[\mathrm{S}_n] = K'_n[\mathrm{S}]^n$, where $K'_n = K_1K_2, ..., K_n$. The mass balance is given by

$$c = [\mathrm{S}] + \sum_{n>1} nK'_n[\mathrm{S}]^n \qquad (10)$$

By solving eq 10 numerically, the concentrations of free solute molecules and *n*-mers can be found. Because the apparent electron mobility $\langle\mu\rangle$ is proportional to the equilibrium fraction of e^-_{solv}, we obtain

$$\frac{\langle\mu_n\rangle}{\langle\mu\rangle} = 1 + \sum_{n>1} K^{(n)}_{\mathrm{eq}}[\mathrm{S}_n] \qquad (11)$$

Two models were examined in which the electron is attached (exclusively) to (i) a trimer or (ii) a tetramer. As seen from Figure 7a, both of these models fit the data well, except for the room-temperature data, which are better accounted for by the tetramer attachment. (This Figure also shows an equilibrium fraction $f_4 = 4[S_4]/c$ of the tetramers.) For methanol at 23 °C, the tetramer also provides the best fit to the data (not shown). The latter result is in agreement with Gangwer et al.,[25] who suggested the tetramer or pentamer as the predominant electron-trapping $(\mathrm{ROH})_n$ cluster for solutions of methanol in *iso*-octane and tetramethylsilane. van't Hoff plots for the equilibrium constants of reaction 3 obtained using these two models are shown in Figure 7b. From these plots, the enthalpy of reaction 3 for $n = 3$ and 4 would be -58 ± 2 and -64.5 ± 2.5 kJ/mol, respectively. Thus, the $(\mathrm{ROH})_n$ trap binds the electron ca. 0.6 eV deeper than the intrinsic solvent trap, and the binding energy E_{t} is ca. 800 meV. Similar estimates were obtained using the approach described in section 4.2.1 by comparison of the activation energies for κ_0 at different ethanol concentrations (Figure 8a). As [EtOH] increases from 0 to 6 to 12 to 25 to 45 mM, these activation energies increase from 32.5 ± 0.5 to 36 ± 0.5 to 45 ± 1.4 to 76 ± 4 to 90 ± 2 kJ/mol. The difference between the first and the last of these energies is ca. -57 ± 3 kJ/mol, which is in a reasonable agreement with the heat of reaction 3 obtained using the van't Hoff analysis. For the methanol tetramer in *iso*-octane, Gangwer et al. estimated this heat to be -63 ± 14 kJ/mol.[25] At 23 °C, K_{eq} for the ethanol tetramer is ca. 65 times greater than for the acetonitrile monomer (Figure 7b).

We turn to electron detachment experiments in which a 1064 nm laser pulse was used to promote the electron from a $\{e^-{:}(\mathrm{ROH})_n\}_{\mathrm{solv}}$ cluster to the CB and observe the subsequent relaxation of the conductivity signal $\Delta\kappa$. The time profile of the $\Delta\kappa$ kinetics does not depend on the delay time t_{L} of the 1064 nm pulse, and the maximum amplitude of the $\Delta\kappa$ signal follows $\kappa_e(t_{\mathrm{L}})$, as is the case for acetonitrile. (Two examples are given in Figure 16S.) In other respects, the $\Delta\kappa$ kinetics are very different from those observed in acetonitrile/*n*-hexane solutions. The most remarkable feature is that the $\Delta\kappa(t)$ kinetics *do not* follow the time profile of the 1064 nm excitation pulse (Figures 9, 10, 17S, and 18S). Even at room temperature (e.g., Figure 17S), there is a "slow" component with a time constant τ_{s} of a several nanoseconds. To analyze these data, the $\Delta\kappa$ kinetics were fit by a weighted sum of (i) a Gaussian with the same $J(t) = (J/\tau_{\mathrm{p}}\sqrt{\pi})\exp(-[(t - t_{\mathrm{L}})/\tau_{\mathrm{p}}]^2)$ profile as that of the 1064 nm excitation pulse (the "spike") and (ii) the same

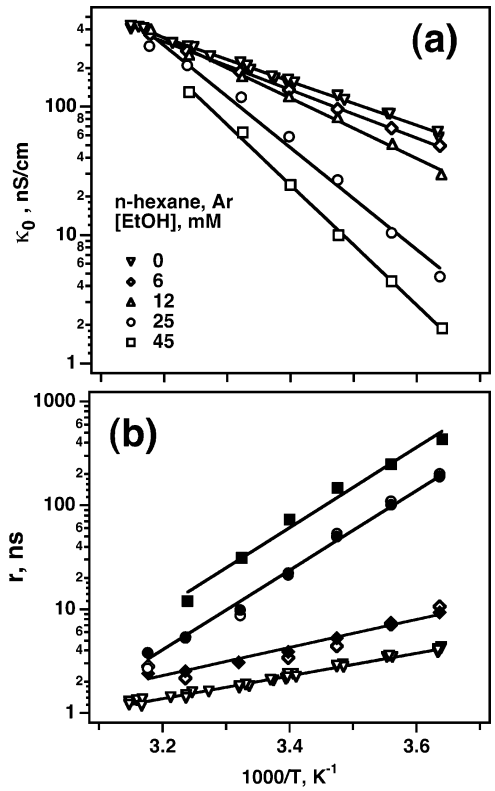

Figure 8. Arrhenius plots for (a) electron conductivity and (b) ratio r (the same excitation conditions as in Figure 5) for ethanol solutions in Ar-saturated *n*-hexane containing 5 μm anthracene as a photosensitizer. The same symbols are used for the same concentrations in each plot: [EtOH] is 0 mM (upturned triangle), 6 mM (diamonds), 12 mM (triangles), 25 mM (circles), and 45 mM (squares). Filled and open symbols in plot b indicate different integration procedures (the same convention used in Figure 5). In plot a, the activation energy increases with the given concentrations as 32.6 ± 0.4, 36 ± 0.5, 44.8 ± 1.4, 76.1 ± 3.6, and 89.7 ± 2 kJ/mol, respectively. The activation energies for the four traces shown in plot b are 20.9 ± 0.4, 25.9 ± 1.7, 73.4 ± 2.4, and 74 ± 5 kJ/mol, respectively (in ascending order with increasing [EtOH]).

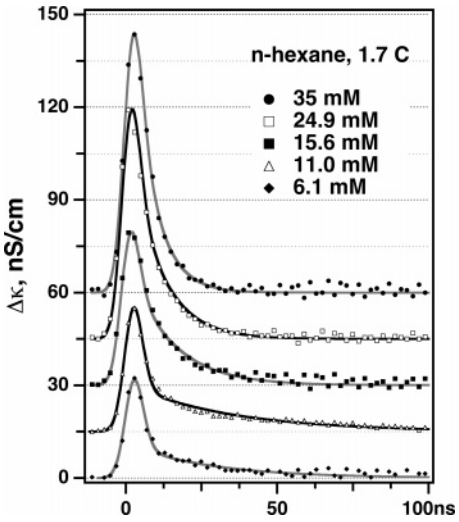

Figure 9. Decay kinetics $\Delta\kappa$ of the conductivity signal induced by the 1064 nm photoexcitation of trapped electrons in Ar-saturated *n*-hexane solution containing 6.1 mM (solid diamonds), 11 mM (open triangles), 15.6 mM (filled squares), 24.9 mM (open squares), and 35 mM (filled circles) ethanol at 1.7 C, using the same excitation conditions as in Figure 5. The kinetics are spaced vertically to facilitate the comparison. The solid lines are least-squares fits to the weighted sum of a Gaussian and the Gaussian convoluted with an exponential.

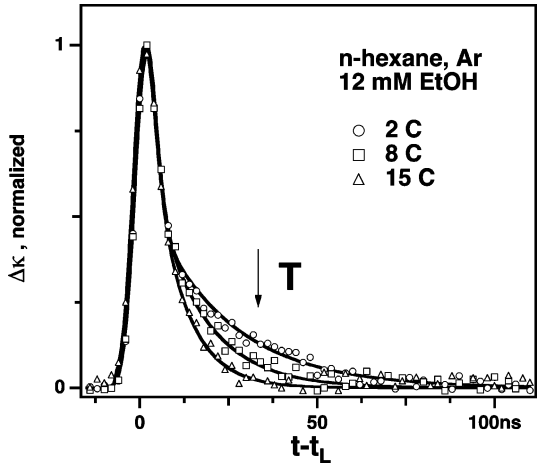

Figure 10. Same as Figure 9 for normalized $\Delta\kappa$ kinetics in 12 mM ethanol in *n*-hexane at three solution temperatures: 1.7 °C (circles), 8.1 °C (squares), and 14.9 °C (triangles).

Gaussian convoluted with $\exp(-t/\tau_s)$. Several examples of such fits are given in Figures 9 and 10. Such an approach can be justified for $J \rightarrow 0$ using the two-trap model (Appendix). At high EtOH concentration, the slow component decays too fast and/or has weight that is too low to be analyzed in this fashion. At lower temperature (Figures 9 and 10), the slow component (with a relative weight approaching 10−50% of the total signal) entirely separates from the initial spike. For [EtOH] < 10 mM, τ_s increases over 20 ns (e.g., Figure 9). With an increase in [EtOH] (Figures 9 and 18S) or in the temperature (Figures 10 and 17Sb), τ_s decreases until the slow component is no longer discernible. The observation of the slow component indicates that the equilibration of the electron between different traps occurs on a time scale that is longer than the duration of the 1064 nm pulse ($\tau_p \approx 4$ ns). At 1.7 °C, this slow equilibration can already be seen in the $\kappa(t)$ kinetics (Figures 12S and 17Sa), which become biexponential (the κ_0 values given in Figure 6 were extrapolated to $t \rightarrow 0$ using the *slower* component, as shown in Figure 12S).

There are two general ways to interpret these observations. First, it can be assumed that the slow component corresponds to the settling of equilibrium reaction 3 that involves a (unique) electron-trapping cluster S_n (e.g., the trimer). As shown in the Appendix, in such a case the time constant $\tau_s \approx (\tau_2 + K\tau_1)/(1 + K)$, where τ_1 and τ_2 are the time constants for thermal emission of the electron from e^-_{solv} and $\{e^-{:}S_n\}_{solv}$ to the CB, respectively, and $K = \langle\mu_n\rangle/\langle\mu\rangle - 1 \approx K^{(n)}[S_n]$. For $K \ll 1$, $\tau_s \rightarrow \tau_2$; for $K \gg \tau_2/\tau_1 \gg 1$, $\tau_s \rightarrow \tau_1$; in the intermediate regime, $\tau_s \approx \tau_2/K$. Thus, if the duration τ_p of the 1064 nm pulse is such that $\tau_1 \ll \tau_p < \tau_2$, for sufficiently low net concentration c of the solute ($K < 10$) the time constant τ_s would behave much as is observed experimentally, provided that τ_2 is 5−30 ns (τ_2 becomes shorter with the increasing temperature). However, further analysis leads to contradiction. Although there is always a slow component for $K \ll 1$, its relative weight is quite small unless $\sigma_2 \ll \sigma_1$ (see the Appendix), where $\sigma_{1,2}$ are the cross sections for photodetachment. If that were the case, the power dependence of ratio r versus J would be almost linear, whereas experimentally it saturates around $J \approx 10^{18}$ photon/cm^2 (Figure 19S). Furthermore, as shown in section 4.1, the *absorptivity* of $\{e^-{:}S_n\}_{solv}$ is certainly *greater* than that of e^-_{solv}, and it may be expected that the detachment cross section would also be larger (unless there is a side photoreaction, such as proton transfer). Last, it seems counterintuitive that τ_2 increases by no more than

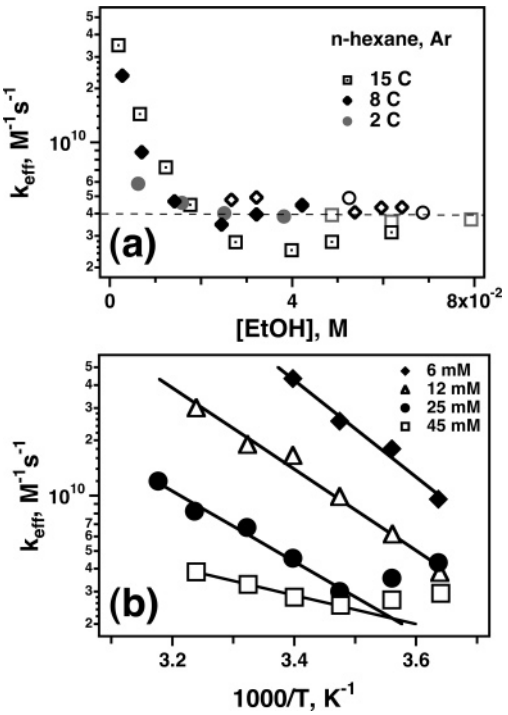

Figure 11. (a) Concentration plots (for fixed temperature) and (b) Arrhenius plots (for fixed concentration) of the effective reaction constant $k_{eff} = (\tau_s c)^{-1}$ corresponding to the slow components in the $\Delta\kappa$ kinetics (Figures 9 and 10). The concentrations and temperatures are indicated in the plots. Filled and open symbols in plot a correspond to different least-squares fitting protocols that differ in the statistical weight given to the slow component.

an order of the magnitude as the binding energy increases from ca. 400 meV (for acetonitrile) to ca. 800 meV (for the alcohol multimer). As pointed out in section 4.1, the simple two-trap model cannot account completely for the observed spectral transformations for electrons in alcohol solutions as a function of solute concentration. The analysis of concentration plots for $\langle\mu\rangle$ given above also suggests that more than one kind of electron-attaching solute trap exists in the solution. The slow component is due to the equilibration between these *solute* traps. Such an equilibration may occur via coupled reactions 3 even if the conversion between $\{e^-{:}S_n\}_{solv}$ species via reaction 5 does not occur; however, as shown below, the experimental observations can be readily rationalized assuming that this dipole coagulation reaction does occur and τ_s is the measure of the corresponding reaction rate. We stress that the treatment is qualitative by necessity because all pertinent parameters for the several interrelated equilibria involved (reactions 3−5) cannot be unambiguously extracted from the data.

Using our estimates for τ_s, the effective bimolecular constant $k_{eff} = (\tau_s c)^{-1}$ can be calculated (Figure 11a and b). Because of the solute speciation via reaction 4, such a "constant" does not relate to any particular reaction (eq 5). Still, for all temperatures between 2 and 23 °C the rate constants k_{eff} for $c > 30$ mM converge to $(3-5) \times 10^9$ M^{-1} s^{-1} (Figure 11a). The activation energy for the solvent viscosity is low (ca. 6.3 ± 0.4 kJ/mol) so that diffusion-controlled reactions in *n*-hexane are weakly activated. The typical rate of such reactions is ca. $(1-5) \times 10^{10}$ M^{-1} s^{-1} (i.e., the apparent rate of reaction that may be responsible for the slow component is a fraction of what one would expect for reaction 5 involving a (normally diffusing) $\{e^-{:}(ROH)_n\}_{solv}$ cluster and a free ROH molecule or a small $(ROH)_m$ cluster). Given that in this concentration range the fraction of the monomers is only 20−50% of the nominal concentration *c* (Figure 1S), the observed equilibration would be consistent with the occurrence of reaction 5 in the solution. As [EtOH] decreases below 20 mM, k_{eff} rapidly increases, reaching 4×10^{10} M^{-1} s^{-1} (for 5 mM ethanol at 15 °C). This increase becomes larger with increasing temperature (Figure 11a). Note that reaction 5 can occur at a higher rate if the $\{e^-{:}S_n\}_{solv}$ species on the left side exhibits high (apparent) mobility.

The Arrhenius plots for k_{eff} at fixed *c* exhibit a large decrease of the activation energy with increasing *c* (Figure 11b). As [EtOH] increases from 6 to 12 to 25 to 45 mM, the activation energy decreases from 50 ± 10 to 42 ± 3 to 34 ± 4 to 15 ± 1 kJ/mol. The low activation energy obtained at the higher end of this concentration range can be explained by the low mobility of the partners in reaction 5: as the reaction rate becomes controlled by (normal) diffusion, the activation energy approaches the activation energy for solvent viscosity. The dramatic increase in the reaction rate in very dilute solutions suggests that a mobile $\{e^-{:}(ROH)_n\}_{solv}$ species is involved. Thus, a large reaction barrier exists for reaction 5 involving the smallest $\{e^-{:}(ROH)_n\}_{solv}$ species (apparently, monomers or dimers) that has large apparent mobility. Although the evidence for the occurrence of direct reaction (eq 5) is not clear-cut, our results suggest that in very dilute solutions the electron equilibria are multistage and take considerable time to settle at the low temperature. This relatively slow settling is chiefly responsible for anomalies in the reaction rates first noticed by Gangwer et al.[25]

In Appendix A of ref 6, we showed that eq 7 would hold regardless of whether reaction 5 occurs, provided that the residence time τ_t in a given trap is appropriately defined. On the strength of this result, one may inquire how this parameter and the ratio *r* change as a function of temperature and concentration. As shown in Figure 6b, for $\chi > 0.01$, $r \propto c^m$ with $m \approx 2.8-2.9$ at all temperatures. Note that as a function of *K* (plotted in Figure 20Sb) the ratio *r* in ethanol solutions behaves very similarly to this ratio in acetonitrile solutions (Figure 4b). For $\chi \approx 0.14$ ethanol solution, *r* increases by 3 orders of magnitude relative to that of neat *n*-hexane. This huge increase swamps the (relatively small) effect of the change in the absorption (photodetachment) cross section with the ethanol concentration (section 4.1) (i.e., most of the increase is due to the increase in the residence time τ_t). Because the exponential parameter *m* is close to 3, the trimer is likely to be the prevalent $\{e^-{:}(ROH)_n\}_{solv}$ species in the solution that is photoexcited by 1064 nm light. The activation energy for *r* does not depend on the ethanol concentration for $c > 20$ mM (Figure 7b). From the Arrhenius plots, the activation energy is ca. 74 ± 5 kJ/mol (770 ± 50 meV). This energy is reasonably close to the binding energy E_t of ca. 800 meV for the trimer (or, possibly, the tetramer) estimated from the van't Hoff plot in Figure 8b.

5. Discussion

5.1. Synopsis. The following picture emerges from our results. In dilute solutions of acetonitrile in *n*-hexane and *iso*-octane ($\chi < 0.01$), a new electron species, $\{e^-{:}MeCN\}_{solv}$, is formed. The binding energy of this species is ca. 0.4 eV (relative to the mobility edge of the CB), which is ca. 0.2 eV greater than the binding energy for the intrinsic electron trap in neat *n*-hexane. The association of the electron with acetonitrile reduces the rate of thermally activated emission into the CB by ca. 200 times versus neat solvent. In the specified concentration range, the solute trap involves a *single* acetonitrile molecule. For *iso*-octane, there is some evidence for nearly irreversible

electron attachment to larger solute clusters and/or delayed formation of molecular anions at higher solute concentration. For λ 1.6 μm, the absorption spectra of trapped electrons in acetonitrile solutions are qualitatively similar to those in neat *n*-hexane, save for less prominent extension toward the visible. As explained in ref 10, the formation of a molecular anion, $MeCN^-$, with a bent C−C−N chain is unlikely, given the low entropy of trapping and unfavorable energetics; furthermore, both theoretical calculations[10,11] and experimental observations[56] indicate that such an anion would not exhibit electron transitions in the infrared. Thus, the electron in the "acetonitrile trap" still resides in the interstitial cavity. The electron is dipole-bound to the CN group of the acetonitrile molecule in the first solvation shell;[10,13] this interaction is mainly electrostatic.

It is commonly assumed[6,7,16] that the rate of thermal emission from electron traps is given by

$$\tau_t^{-1} \approx \nu_t \exp-(E_t/k_BT) \qquad (12)$$

where ν_t is the attempt-to-escape frequency ($10^{12}-10^{15}$ Hz or $\sim E_t/h$),[16] E_t is the binding energy, and k_BT is the thermal energy (ca. 25.4 meV at 23 °C). Simple-minded use of this equation indicates that the thermal emission from $\{e^-$:MeCN$\}_{solv}$ should be 3000 times slower than that from e^-_{solv}, whereas experimentally it is only 200 times slower. Furthermore, for both of these electron traps, the frequency ν_t (7×10^{15} and 3×10^{14} Hz, respectively) is unrealistically large. We conclude that eq 12 overestimates the stability of electron traps in mixed solvents: something other than energetics controls this stability. The most likely cause is the loss of a solute molecule via backward reaction 5: the entropy factor prevents substitution in the solvation shell of the cavity electron. As shown by previous workers[20−26] and confirmed in this study (section 4.2.2), the $\{e^-$:ROH$\}_{solv}$ species, for which the interaction with the electron is relatively weak, is thermodynamically unstable, whereas the binding energy for this species can only be higher than that for e^-_{solv}. Apparently, the entropy term prevails for this species: it either loses the ROH molecule or undergoes proton transfer.

For larger alcohol clusters, the situation is different because the electron can interact with several OH groups, and the binding energies are large. The same behavior was observed for methanol, ethanol, and 1-propanol. Our data point to the alcohol trimer or tetramer as the predominant form of the cluster that reversibly traps electron via reactions 2 and 3 for $\chi < 0.015$, with a binding energy of 770 or 800 meV (section 4.2.2). Despite this large binding energy, the free energy of reaction 3 for these multimers is only 100 meV greater than that for the acetonitrile monomer with $E_t \approx 400$ meV. Surprisingly, photodetachment experiments using infrared light give no evidence for a larger $\{e^-$:$(ROH)_n\}_{solv}$ species postulated to account for *irreversible* electron scavenging (section 1S).[20−25] Instability of the ground and/or excited state of these species toward proton transfer and the onset of bound-to-bound s → p transition bond is one possible explanation for this unexpected observation. The size of the dominant electron trapping solute cluster appears to be tightly constrained, both from below and above, over a wide concentration range. Previous studies seem to support this conclusion. For example, Smirnov et al.[26] studied ODMR spectra from dilute ethanol/squalane solutions at 23 °C and observed no change in the shape of the resonance line of solvated electrons as [EtOH] increased from 10 to 100 mM. As seen from Figure 2a in section 4.1, the TA spectra of electrons in ethanol/*n*-hexane solutions can be understood, to a first approximation, in terms of just two species contributing to the spectrum. All of these observations point to a relative uniformity of trapped-electron species at thermodynamic equilibrium in dilute alcohol solutions. The dipole coagulation and electron attachment do not yield metastable $\{e^-$:$(ROH)_n\}_{solv}$ species beyond a certain size.

Another intriguing observation is the possible occurrence of reaction 5, which could account for the slow settling of electron equilibria on the nanosecond time scale in very dilute solutions ($\chi < 5 \times 10^{-3}$) at low temperature. Previous researchers believed that electron equilibria are settled very rapidly, and this is indeed the case for concentrated, room-temperature alcohol solutions. For example, Kenney-Wallace and Jonah[19] concluded that for $\chi > 0.03-0.05$ (which is well above the concentration range where dipole coagulation on the nanosecond time scale occurs) all equilibria (eq 3) are settled within 30 ps. Gangwer et al.[25] estimated that methanol multimers ($n \geq 4$) in *iso*-octane attach an electron with a rate constant $>10^{12}$ M^{-1} s^{-1}. However, neither group considered the possibility that the trap, once filled, can incorporate more solvent molecules or exchange the electron with a larger cluster. Our results suggest that such reactions (dipole coagulation)[18] do occur in very dilute solutions. Apparently, reaction 5 involves a monomer or a dimer. The reaction is slow and thermally activated, suggesting a substantial barrier toward the inclusion of the alcohol molecule in the solvation shell of the $\{e^-$:$(ROH)_n\}_{solv}$ species.

5.2. Structure of the $\{e^-$:$S_n\}_{solv}$ Species. Because the interaction of the electron and polar molecules in the solvation shell of $\{e^-$:$S_n\}_{solv}$ is mainly electrostatic, it would be natural to use the so-called "dielectric continuum" models for electron solvation[2c,57] to model its structure. In this class of models, a few fixed dipoles are treated explicitly in the interaction Hamiltonian; the rest of the solvent, beyond some cutoff radius, is treated as a continuum with bulk dielectric properties. Gangwer et al.[25] used such an approach to estimate the energetics of electron trapping by methanol multimers in *iso*-octane. Unfortunately, this model makes no provision for the involvement of *solvent* molecules, whereas such an involvement is certainly important.

Because a self-consistent theory of solvated electron in alkanes is presently lacking,[6] below we use the simplest (Wigner-Seiz cell) model of such an electron species:[6,58,59] the s electron wave function $\Psi_s(r)$ occupying a spherical potential well with hard core radius a and depth U (measured relative to the CB edge at V_0). The binding energy E_t of the electron is a function of the depth U; the plot of this function for $a = 3.5$ Å is shown in Figure 12a. The latter estimate for the radius is supported by simulations of optical spectra in liquid[6,45] and vitreous[58] alkanes, magnetic resonance spectroscopy,[8b] and dc conductivity measurements at high pressure;[7a] this estimate is also compatible with the current microscopic theories of electron trapping in dense simple liquids[60] and amorphous polyethylene.[61] The critical well depth $U_c = \pi^2\hbar^2/8m_ea^2$ (where m_e is the electron mass and $\hbar$ is the Planck constant) for $a = 3.5$ Å is ca. 770 meV; for $U < 4U_c$, only one bound state exists; for $U < U_c$, no bound state exists.[59] In neat *n*-alkane liquids, $E_t/U_c \approx 0.2-0.3$ and only *bound-to-continuum* transitions are possible. The well depth $U \approx V_0 - E_{pol}$, where E_{pol} is the polarization energy and V_0 is the energy of e^-_{qf} versus vacuum.[6,7] The polarization energy can be crudely estimated using the Born equation, $E_{pol} \approx -(1 - \epsilon^{-1})e^2/2a$, where e is the elementary charge and ϵ is the bulk dielectric constant.[6] Apparently, this equation gives too low an estimate because the polarizability of C−C bonds in the groups lining the solvation cavity appears

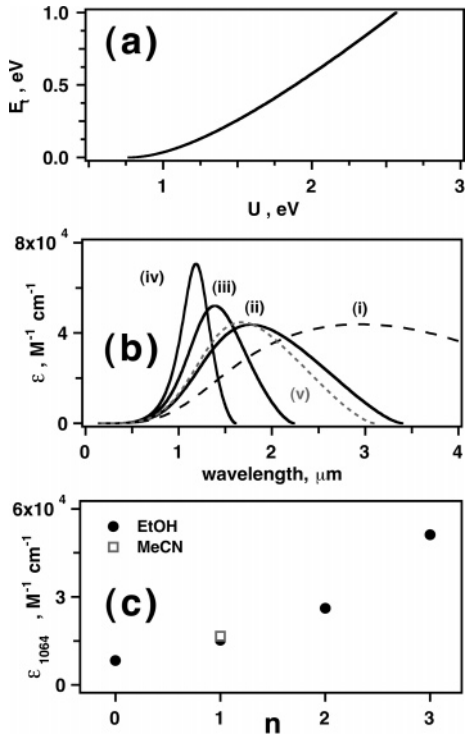

Figure 12. Theoretical simulations using a spherical well model with a hard core well radius of $a = 3.5$ Å. (a) Dependence of the binding energy E_t of the trap on the interaction potential U inside the well. (b) Simulated absorption spectra for (i) e^-_{solv} in neat *n*-hexane, (ii−iv) ethanol clusters in *n*-hexane ($(e^-{:}S_n)_{solv}$ with $n = 1-3$, respectively), and (v) $(e^-{:}MeCN)_{solv}$. Simulation parameters are given in the text. (c) Plot of the molar extinction coefficient for the trapped electron at 1 μm vs the number of "attached" EtOH (filled circles) and MeCN (open squares) molecules in the first solvation shell (the same calculation as in plot b).

to be several times greater than that in the bulk liquid.[6,8a,58c] For $r > a$, the radial wave function $\Psi_s(r)$ of the ground state decreases exponentially toward the bulk as $r\Psi(r) \propto \exp(-r/r_{loc})$, where $r_{loc} \approx 2a\pi^{-1}[U_c/E_t]^{1/2}$ is the localization radius.[58a,59] In neat alkanes, this radius is 4−5 Å (i.e., the extension of the electron density onto the solvent is substantial). In this respect, e^-_{solv} in alkanes is different from the electron in polar solvents, where the binding energy is large, the electron wave function is confined inside the cavity, and bound-to-bound s → p transitions dominate in the visible and in the infrared.[2,4,54] In polar solvents, the cavity radius a rapidly increases with increasing temperature.[31,32] For alkanes, this radius is nearly constant;[6,7a,58] E_{pol} also depends weakly on the temperature. However, U (and, consequently, E_t) decreases rapidly with increasing temperature because the energy V_0 of e^-_{qf} increases greatly with solvent density.[6,7a] The latter changes substantially as a function of temperature for alkane solvents. In ref 6, the absorption spectra of e^-_{solv} in liquid *n*-hexane were fit using the spherical well model, and binding energies E_t were estimated at several temperatures; these estimates are in good agreement with the activation energies of thermal emission obtained from dc conductivity experiments. For neat *n*-hexane at 23 °C, $E_t \approx$ 200 meV, $U \approx 1.39$ eV, and the absorption maximum for the bound-to-continuum transition is at $\lambda \approx 2.95$ μm (Figure 12b, trace i).[6,45]

The same spherical well model can be used to estimate the binding energies for $\{e^-{:}S_n\}_{solv}$ species. To this end, we assumed that the "mean" well depth U increases stepwise relative to the same quantity U_n for the intrinsic solvent trap by the energy V_{dip} of interaction with a polar molecule. The latter energy is estimated using the point dipole approximation. All solute molecules are equivalent so that $U = U_n + \langle n\rangle V_{dip}$. We further assumed that the cavity size does not change upon the inclusion of these solute molecules.

Let us consider first the acetonitrile monomer. As suggested in section 5.1, the cavity electron is solvated by the methyl group with the CN group pointing away from the cavity center. Assuming that the methyl protons are at the hard core radius $r \approx a$, the center of the CN bond is ca. 6 Å away from the cavity center. The interaction energy V_{dip} for the 3.92 D dipole in the cyano group is ca. 330 meV, which gives $U \approx 1.72$ eV and $E_t \approx 390$ meV. This binding energy compares favorably with the 400 meV obtained experimentally (section 4.2.1). Figure 12b, trace v shows the simulation of the absorption spectrum for the 390 meV trap. The absorption maximum is at $\lambda \approx 1.68$ μm, which is just beyond the observation range of our pulse radiolysis−TA setup ($\lambda < 1.6$ μm, section 4.1). The absorptivity at $\lambda = 1$ μm is ca. 2 times that for the $E_t \approx 200$ meV trap, in reasonable agreement with experiment. For $\lambda <$ 1.6 mm, the spectral profiles for 200 and 400 meV traps are similar, with the shallower trap exhibiting less sloping toward the blue. This is also in agreement with experiment (Figure 1a).

For alcohol clusters, the same method can be used to solve the inverse problem: estimating the mean distances to OH dipoles from the energetics. The binding energy E_t for the prevalent ethanol multimer is ca. 770 meV (from the activation energy of electron photodetachment in Figure 8b) or 800 meV (from van't Hoff plots in Figure 7). Using the plot in Figure 12a, we find that U of 2.27 or 2.31 eV would correspond to these binding energies so that $V_{dip} \approx 880/\langle n\rangle$ meV, where $\langle n\rangle$ is the mean number of solute molecules in the solvation shell of the cavity electron. Placing the center of a radially aligned OH dipole (ca. 1.7 D) at a distance r_{OH} from the cavity center, we find that $r_{OH} \approx 4.2$ Å for $\langle n\rangle = 3$ and $r_{OH} \approx 4.8$ Å for $\langle n\rangle = 4$. Because the O−H bond length is ca. 1 Å, the trimer gives a better match, with the OH dipoles at an angle to the radial direction. Such an arrangement is in accord with quantum mechanical−molecular dynamics models of the solvated electron in neat water and alcohols.[4,54] The monomer and the dimer are predicted to have binding energies of 365 and 555 meV, respectively, with their absorption bands centered at 1.78 and 1.39 μm, respectively (Figure 12b, traces ii−iv). The trimer ($E_t \approx 770$ meV) is calculated to have maximum absorbance at $\lambda \approx 1.18$ μm; the molar absorptivity at $\lambda = 1$ μm is ca. 6.2 times greater than that for e^-_{solv} ($E_t \approx 200$ meV; Figure 12c). This estimate is in agreement with the factor of ca. 5 obtained experimentally (section 4.1). At the higher end of the concentration range explored (ca. 120 mM), at which the conductivity signal is dominated by a single reversibly trapped species, the TA spectrum peaks at 0.95−1 μm (Figure 2a). This position is in a reasonable agreement with the estimate given above. Whereas our approach is obviously crude, it yields reasonable estimates for the energetics observed. Improving this model is hindered by the lack of microscopic insight into the nature of *solvent* traps in liquid alkanes.

6. Conclusions

Electron localization in dilute ($\chi < 0.015$) solutions of polar molecules in nonpolar liquids has been studied using TA spectroscopy and conductivity. In the conductivity experiments, 1.17 eV photon excitation was used to detach the electron from a $\{e^-{:}S_n\}_{solv}$ species and observe relaxation dynamics on the nanosecond time scale. In acetonitrile solutions, the elec-

tron can attach to a single solute molecule forming the $\{e^-$:MeCN$\}_{solv}$ species. The dynamics of this attachment can be understood using a simple two-trap model. The binding energy for this $\{e^-$:MeCN$\}_{solv}$ species is ca. 400 meV, and its lifetime (limited by thermal emission to the conduction band) is ca. 1 ns at 23 °C. The properties of this electron species can be rationalized assuming that MeCN substitutes for the solvent molecules in the first solvation shell of e^-_{solv}. The methyl group of MeCN is at the cavity wall, whereas the C−N group is ca. 6 Å away from the center of the solvation cavity and points outward. The resulting structure is midway between the solvated electron in neat alkanes[6,7,16,17,58] and in liquid acetonitrile.[10−14] Further inclusion of acetonitrile molecules does not occur, most likely because of the formation of a covalently bound dimer anion with lower energy.[10,11,14,56] Interestingly, thermal emission from the acetonitrile monomer trap (as well as from the related ethanol monomer trap) appears to be much faster than expected from the energetics alone (section 5.1). Apparently, entropy plays as much a role as the binding energy in determining the stability of these solute traps. For example, while the binding energy for the $\{e^-$:ROH$\}_{solv}$ species is ca. 165 meV greater than this energy for e^-_{solv} (section 5.2), the electron equilibrium is completely shifted toward the shallower trap. The driving force of electron attachment to the ethanol *tetramer* is only 0.1 eV more negative than that for the acetonitrile *monomer*.

Electron trapping in dilute alcohol solutions is more involved because dipole coagulation (reaction 5) occurs concurrently with several electron and H-bonding equilibria (reactions 3 and 4, respectively). The resulting dynamics are rather complex, and we were unable to disentangle all reactions involved. Still, several conclusions can be reached. The electron does not attach to the alcohol monomer. This is due to both unfavorable thermodynamics (because the resulting species is unstable toward the reverse reaction) and the occurrence of proton transfer (reaction 8). The latter reaction probably occurs for other $\{e^-$:$(ROH)_n\}_{solv}$ species. Its rapid occurrence (either in the ground or in the excited states) for higher $\{e^-$:$(ROH)_n\}_{solv}$ multimers that attach the electron *irreversibly* might account for the lack of IR-light-induced electron detachment from these species (section 1S). The lower multimers ($n < 5$) attach the electron *reversibly*. Following initial attachment reaction 3, dipole coagulation reaction 5 is observed on the nanosecond time scale. When equilibrium is reached, the prevalent $\{e^-$:$(ROH)_n\}_{solv}$ species ($n \approx 3, 4$) binds the electron by ca. 800 meV. These energetics and the TA spectra observed are consistent with the OH groups of solute molecules lining the solvation cavity.

This study was conceived as a search for condensed-matter analogues of dipole-bound[62] and cluster[2b,12,13,63,64] anions occurring in the gas phase. In recent years, cluster anions of polar molecules, such as $(H_2O)_n^-$, have been extensively studied (see refs 2b, 63, and 64 and references therein). Such clusters are interesting in their own right but also as model systems for electron solvation in the bulk liquid. Because surface trapping prevails in small and even medium-size clusters ($n < 20$),[2b,64] a direct comparison between these cluster anions and e^-_{solv} in liquids is difficult, although possible.[64] However, electron trapping in large clusters ($n > 25-50$) where internal localization prevails is as difficult to model as that in neat liquids. The $\{e^-$:$S_n\}_{solv}$ species occurring in alkanes provide what these small gas-phase S_n^- clusters do not: a model system for e^-_{solv} in a neat polar liquid with few polar molecules directly involved. This, in turn, suggests that a species whose anion core closely resembles the first solvation shell of e^-_{solv} in a polar liquid may be achieved in the gas phase by making a composite cluster anion in which several polar molecules are embedded in a large number of nonpolar molecules. Perhaps "solvents" for which V_0 (the energy of the quasi-free electron relative to vacuum) is small and electron trapping is facile (e.g., *n*-alkanes other than methane) would be most suitable. The resulting $\{e^-$:$S_n\}_{solv}$ species has the same structure and energetics regardless of the alkane solvent (section 4).

Our study also hints at the possibility of a fixed-geometry molecular cage "solvating" the electron in an alkane solution. Such a cage (by analogy to alcohol multimers in *n*-hexane) would include several radial groups assembled around the central cavity. Crown ethers and their aza derivatives, cryptands, and cyclosiloxanes provide a structural motif conducive to electron trapping in this fashion. There are precedents for fixed-geometry e^-_{solv} species in low-temperature crystalline solids: single crystals of sugars[65] and hexagonal ice[66] are known to trap electrons because of the fortuitous orientation of OH groups at certain interstitial sites. Another example is electrides (e.g., Cs^+[18-crown-6]$\cdot e^-$)[67] that (presumably) trap electrons in cavities and channels. Arguably, electrons "solvated" by well-defined cages would constitute an ideal condensed-phase model for solvated electrons in polar liquids because their fixed geometry would make ab initio modeling much easier and their properties would be less dependent on solvent fluctuations.

Acknowledgment. I.A.S. thanks C. D. Jonah, R. A. Holroyd, and A. Mozumder for many useful discussions. This work was supported by the Office of Science, Division of Chemical Sciences, US-DOE under contract number W-31-109-ENG-38.

Supporting Information Available: A single pdf file containing (1) an appendix of the two-trap model; (2) a section on irreversible trapping; and (3) Figures 1S to 22S with captions. This material is available free of charge via the Internet at http://pubs.acs.org.

References and Notes

(1) Shkrob, I. A.; Sauer, M. C., Jr. In *Charged Particle and Photon Interactions with Matter*; Mozumder, A., Hatano, Y., Eds.; Marcel Dekker: New York, 2004; p 301.

(2) (a) Hart, E. J.; Anbar, M. *The Hydrated Electron*; Wiley-Interscience: New York, 1970. (b) Coe, J. V. *Int. Rev. Phys. Chem.* **2001**, *20*, 33. (c) Kevan, L. *Adv. Radiat. Chem.* **1974**, *4*, 181.

(3) Tauber, M. J.; Mathies, R. A. *Chem. Phys. Lett.* **2002**, *354*, 518.Tauber, M. J.; Mathies, R. A. *J. Phys. Chem. A* **2001**, *105*, 10952. Tauber, M. J.; Mathies, R. A. *J. Am. Chem. Soc.* **2003**, *125*, 1394. (b) Dikanov, S. A.; Tsvetkov, Y. D. *Electron Spin−Echo Envelope Modulation (ESEEM) Spectroscopy*; CRC Press: Boca Raton, FL, 1992.

(4) (a) Rossky, P. J.; Schnitker, J. *J. Phys. Chem.* **1988**, *92*, 4277. Schnitker, J.; Motakabbir, K.; Rossky, P. J.; Friesner, R. A. *Phys. Rev. Lett.* **1988**, *60*, 456. Webster, F. J.; Schnitker, J.; Frierichs, M. S.; Friesner, R. A.; Rossky, P. J. *Phys. Rev. Lett.* **1991**, *66*, 3172. Webster, F. J.; Rossky, P. J.; Friesner, R. A. *Comput. Phys. Commun.* **1991**, *63*, 494. Motakabbir, K.; Schnitker, J.; Rossky, P. J. *J. Chem. Phys.* **1992**, *97*, 2055. Rosenthal, S. J.; Schwartz, B. J.; Rossky, P. J. *Chem. Phys. Lett.* **1994**, *229*, 443. Murphrey, T. H.; Rossky, P. J. *J. Chem. Phys.* **1993**, *99*, 515. Schwartz, B. J.; Rossky, P. J. *J. Chem. Phys.* **1994**, *101*, 6917. Schwartz, B. J.; Rossky, P. J. *J. Phys. Chem.* **1994**, *98*, 4489. Schwartz, B. J.; Rossky, P. J. *Phys. Rev. Lett.* **1994**, *72*, 3282. Schwartz, B. J.; Rossky, P. J. *J. Chem. Phys.* **1994**, *101*, 6902. Wong, K. F.; Rossky, P. J. *J. Phys. Chem. A* **2001**, *105*, 2546. (b) Borgis, D.; Staib, A. *Chem. Phys. Lett.* **1994**, *230*, 405. Staib, A.; Borgis, D. *J. Chem. Phys.* **1995**, *1995*, 2642. Borgis, D.; Staib, A. *J. Chim. Phys.* **1996**, *39*, 1628. Borgis, D.; Staib, A. *J. Chem. Phys.* **1996**, *104*, 4776. Borgis, D.; Staib, A. *J. Phys.: Condens. Matter* **1996**, *8*, 9389. Staib, A.; Borgis, D. *J. Chem. Phys.* **1996**, *104*, 9027. Borgis, D.; Bratos, S. *J. Mol. Struct.* **1997**, *1997*, 537. Nicolas, C.; Boutin, A.; Levy, B.; Borgis, D. *J. Chem. Phys.* **2003**, *118*, 9689. (b) Boero, M.; Parrinello, M.; Terakura, K.; Ikeshoji, T.; Liew, C. C. *Phys. Rev. Lett.* **2003**, *90*, 226403.

(5) Son, D. H.; Kambhampati, P.; Kee, T. W.; Barbara, P. F. *Chem. Phys. Lett.* **342**, *2001*, 571. Son, D. H.; Kambhampati, P.; Kee, T. W.; Barbara, P. F. *J. Phys. Chem. A* **2001**, *105*, 8269.

(6) Shkrob, I. A.; Sauer, M. C., Jr. *J. Chem. Phys.* **2005**, *122*, 134503.
(7) (a) Holroyd, R. A. In *Charged Particle and Photon Interactions with Matter*; Mozumder, A., Hatano, Y., Eds.; New York, 2004; pp 175. Holroyd, R. A.; Schmidt, W. F. *Annu. Rev. Phys. Chem.* **1989**, *40*, 439. (b) Schmidt, W. F. *Can. J. Chem.* **1977**, *55*, 2197. Schmidt, W. F. *IEEE Trans. Electron. Insul.* **1984**, *EI-19*, 389. Schmidt, W. F. *Rev. Phys. Appl.* **1987**, *22*, 1113. (c) Warman, J. M. In *The Study of Fast Processes and Transient Species by Electron-Pulse Radiolysis*; Baxendale, J. H., Busi, F., Eds.; Reidel: Amsterdam, The Netherlands, 1982; p 433. (d) Yakovlev, B. S.; Lukin, L. V. *Adv. Chem. Phys.* **1985**, *60*, 99.
(8) (a) Kevan, L. *J. Phys. Chem.* **1978**, *82*, 1144. Kimura, T.; Fueki, K.; Narayana, P. A.; Kevan, L. *Can. J. Chem.* **1977**, *55*, 1940. (b) Kevan, L.; Ichikawa, T.; Ichikawa, T. *J. Phys. Chem.* **1980**, *84*, 3260. Narayana, P. A.; Kevan, L. *J. Chem. Phys.* **1976**, *65*, 3379.
(9) Nishida, M. *J. Chem. Phys.* **1977**, *65*, 242.
(10) Shkrob, I. A.; Sauer, M. C., Jr. *J. Phys. Chem. A* **2002**, *106*, 9120.
(11) Xia, C.; Peon, J.; Kohler, B. *J. Chem. Phys.* **2002**, *117*, 8855.
(12) Mitsui, M.; Ando, N.; Kokubo, S.; Nakajima, A.; Kaya, K. *Phys. Rev. Lett.* **2003**, *91*, 153002.
(13) Takayanagi, T. *Chem. Phys.* **2004**, *302*, 85.
(14) Bell, I. P.; Rodgers, M. A. J.; Burrows, H. D. *J. Chem. Soc.* **1976**, 315.
(15) Munoz, R. C. In *Excess Electrons in Dielectric Media*; Ferradini, C., Jay-Gerin, J.-P., Eds.; CRC Press: Boca Raton, FL, 1991; p 161. Munoz, R. C. *Radiat. Phys. Chem.* **1988**, *32*, 169.
(16) Mozumder, A. *Res. Chem. Intermed.* **1999**, *25*, 243. Mozumder, A. *Chem. Phys. Lett.* **1993**, *207*, 245. Mozumder, A. *Chem. Phys. Lett.* **1995**, *233*, 167. Mozumder, A. *J. Phys. Chem.* **1996**, *100*, 5964.
(17) Berlin, Y. A.; Nyikos, L.; Schiller, R. *J. Chem. Phys.* **1978**, *69*, 2401.
(18) Mozumder, A. *J. Phys. Chem.* **1972**, *76*, 3824.
(19) Kenney-Wallace, G. A.; Jonah, C. D. *J. Phys. Chem.* **1982**, *86*, 2572.
(20) Baxendale, J. H. *Can. J. Chem.* **1977**, *55*, 1996.
(21) Baxendale, J. H.; Sharpe, P. H. G. *Chem. Phys. Lett.* **1976**, *41*, 440.
(22) Ahmad, M. S.; Atherton, S. J.; Baxendale, J. H. *Radiat. Res., Proc. Int. Congr., 6th*; **1979**, 220.
(23) Baxendale, J. H.; Rasburn, E. J. *J. Chem. Soc., Faraday Trans. 1* **1974**, *70*, 705.
(24) Baxendale, J. H.; Keene, J. P.; Rasburn, E. J. *J. Chem. Soc., Faraday Trans. 1* **1974**, *70*, 718.
(25) Gangwer, T. E.; Allen, A. O.; Holroyd, R. A. *J. Phys. Chem.* **1977**, *81*, 1469.
(26) Smirnov, S. N.; Anisimov, O. A.; Molin, Y. N. *Chem. Phys.* **1986**, *109*, 321.
(27) Ito, M.; Kimura, T.; Fueki, K. *Can. J. Chem.* **1981**, *59*, 2803. Kimura, T.; Hirao, K.; Okabe, N.; Fueki, K. *Can. J. Chem.* **1984**, *62*, 64.
(28) Stokes, R. H. *J. Chem. Soc., Faraday Trans. 1* **1977**, *73*, 1140. Smith, F.; Brown, I. *Aust. J. Chem.* **1973**, *26*, 691.
(29) Michel, H.; Lippert, E. In *Organic Liquids*; Buckingham, A. D., Lippert, E., Bratos, S., Eds.; Wiley: New York, 1978; p 293; see also p 13.
(30) (a) Whittenburg, S. L.; Wang, C. H. *J. Chem. Phys.* **1977**, *66*, 4255. (b) Knozinger, K.; Leutloff, D.; Wittenbeck, R. *J. Mol. Struct.* **1980**, *60*, 115. (c) Kovacs, H.; Kowalewski, J.; Maliniak, A.; Stilbs, P. *J. Phys. Chem.* **1989**, *93*, 962. (d) Strizhakova, N. G.; Shevchenko, Yu. B.; Trachevski, V. V.; Kozachkov, S. G.; Maletin, Yu. A. *Ukr. Chem. J.* **1997**, *63*, 26. (e) Kratochwill, V. A.; Weidner, J. U.; Zimmermann, H. *Ber. Bunsen-Ges. Phys. Chem.* **1973**, *77*, 408.
(31) Jortner, J.; Gaathon, A. *Can. J. Chem.* **1977**, *55*, 1801.
(32) Bartels, D. M.; Takahashi, K.; Cline, J. A.; Marin, T. W.; Jonah, C. D. *J. Phys. Chem. A* **2005**, *109*, 1299.
(33) Shkrob, I. A.; Sauer, M. C., Jr. *J. Phys. Chem. B* **2001**, *105*, 7027. Shkrob, I. A.; Sauer, M. C., Jr. *J. Phys. Chem. B* **2001**, *105*, 4520.
(34) Shkrob, I. A.; Sauer, M. C.; Trifunac, A. D. In *Radiation Chemistry: Present Status and Future Trends*; Jonah, C. D., Rao, B. S. M., Eds.; Elsevier: Amsterdam, 2001; p 175.
(35) Mehnert, R.; Brede, O.; Naumann, W. *J. Radioanal. Nucl. Chem. A* **1986**, *101*, 307. Mehnert, R. In *Radical Ionic Systems*; Lund, A., Shiotani, M., Eds.; Kluwer: Amsterdam, 1991; p 231.
(36) Le Motais, B. C.; Jonah, C. D. *Radiat. Phys. Chem.* **1989**, *33*, 505. Lewis, M.; Jonah, C. D. *Radiat. Phys. Chem.* **1989**, *33*, 1. Trifunac, A. D.; Werst, D. W.; Percy, L. T. *Radiat. Phys. Chem.* **1989**, *34*, 547.
(37) Sauer, M. C., Jr.; Werst, D. W.; Jonah, C. D.; Trifunac, A. D. *Radiat. Phys. Chem.* **1991**, *37*, 461. See also Tagawa, S.; Hayashi, N.; Yoshida, Y.; Washio, M.; Tabata, Y. *Radiat. Phys. Chem.* **1989**, *34*, 503.
(38) Shkrob, I. A.; Sauer, M. C., Jr.; Trifunac, A. D. *J. Phys. Chem.* **1996**, *100*, 7237.
(39) Wojnarovits, L. In *Charged Particle and Photon Interactions with Matter*; Mozumder, A., Hatano, Y., Eds.; Marcel Dekker: New York, 2004; p 365.
(40) Stass, D. V.; Sviridenko, F. B.; Molin, Yu. N. *Radiat. Phys. Chem.* **2003**, *67*, 207.
(41) Shkrob, I. A.; Trifunac, A. D. *Radiat. Phys. Chem.* **1995**, *46*, 83.
(42) Zhang, T.; Lee, Y. J.; Kee, T. W.; Barbara, P. F. *Chem. Phys. Lett.* **2005**, *403*, 257.
(43) Sander, M. U.; Brummund, U.; Luther, K.; Troe, J. *J. Phys. Chem.* **1993**, *97*, 8378. Siebbeles, L. D. A.; Emmerichs, U.; Hummel, A.; Bakker, H. J. *J. Chem. Phys.* **1997**, *107*, 9339. Long, F. H.; Lu, H.; Eisenthal, K. B. *J. Phys. Chem.* **1995**, *99*, 7436.
(44) *CRC Handbook of Radiation Chemistry*; Tabata, Y., Ito, Y., Tagawa, S., Eds.; CRC Press: Boca Raton, FL, 2000; Table V.6 and Chapter V.C.2, p 305.
(45) Atherton, S. J.; Baxendale, J. H.; Busi, F.; Kovacs, A. *Radiat. Phys. Chem.* **1986**, *28*, 183.
(46) Shkrob, I. A.; Sauer, M. C., Jr.; Jonah, C. D.; Takahashi, K. *J. Phys. Chem. A* **2002**, *106*, 11855.
(47) Sviridenko, F. B.; Stass, D. V.; Molin, Yu. N. *Mol. Phys.* **2003**, *101*, 1839 (depr alcohols).
(48) The conductivity signal depends on both the electron mobility and the electron concentration; the latter quantity is temperature-dependent but is the same with and without the acetonitrile, as seen from the constancy of the long-time ion conductivity as a function of [MeCN].
(49) In neat *n*-hexane,[6] this is not the case because of the formation of an impurity anion that absorbs 1064 nm light. In acetonitrile and alcohol solutions, this impurity is not formed because of the competitive trapping/scavenging.
(50) Lukin, L. V.; Tolmachev, A. V.; Yakovlev, B. S. *High Energy Chem.* **1983**, *16*, 325. Lukin, L. V.; Tolmachev, A. V.; Yakovlev, B. S. *High Energy Chem.* **1987**, *21*, 357. Lukin, L. V. *J. Photochem. Photobiol., A* **1998**, *112*, 111. Brazgun, F. F.; Nadtochenko, V. A.; Rubtsov, I. V.; Lukin, L. V. *Chem. Phys.* **1996**, *211*, 469. Lukin, L. V.; Balakin, A. A. *Chem. Phys.* **2001**, *265*, 87.
(51) There were previous reports of a large effect of alcohols on the ion mobility in *n*-alkanes; see Adamczewski, I. *Ionization, Conductivity and Breakdown in Dielectric Liquids*; Taylor & Francis: London; 1965; p 205. To our knowledge, no explanation has been given for these observations. Almost certainly, this decrease is due to the clustering of alcohol molecules around the anion, which forms strong H bonds with the solute. (See, for example, Mautner, M. *Chem. Rev.* **2005**, *105*, 213.) This effect is interesting in its own right; however, it has not been pursued in the present study.
(52) With the Hudson method used by Gangwer et al.,[25] it is the $k/\langle\mu\rangle$ ratio that is actually determined.
(53) *CRC Handbook of Radiation Chemistry*; Tabata, Y., Ito, Y., Tagawa, S., Eds.; CRC Press: Boca Raton, FL, 2000; Table VII.6, p 416.
(54) Turi, L. *J. Chem. Phys.* **1999**, *110*, 10364. Turi, L.; Mosyak, A.; Rossky, P. J. *J. Chem. Phys.* **1997**, *107*, 1970. Tauber, M. J.; Stuart, C. M.; Mathies, R. A. *J. Am. Chem. Soc.* **2004**, *126*, 3414. Narayana, M.; Kevan, L. *J. Chem. Phys.* **1980**, *72*, 2891.
(55) Silva, C.; Walhout, P. K.; Reid, P. J.; Barbara, P. F. *J. Phys. Chem. A* **1998**, *102*, 5701. Walhout, P. K.; Alfano, J. C.; Kimura, Y.; Silva, C.; Reid, P. J.; Barbara, P. F. *Chem. Phys. Lett.* **1995**, *232*, 135. Kenney-Wallace, G. A.; Hall, G. E.; Hunt, L. A.; Sarantidis, K. *J. Phys. Chem.* **1980**, *84*, 1145.
(56) Shkrob, I. A.; Takeda, K.; Williams, F. *J. Phys. Chem. A* **2002**, *106*, 9132. Williams F.; Sprague, E. D. *Acc. Chem. Res.* **1982**, *15*, 408. Bonin, M. A.; Chung, Y. J.; Sprague, E. D.; Takeda, K.; Wang, J. T.; Williams, F. *Nobel Symp.* **1972**, *22*, 103.
(57) See, for example, Jortner, J. *Ber. Bunsen-Ges. Phys. Chem.* **1971**, *75*, 696. Fueki, K.; Narayana, P. A.; Kevan, L. *J. Chem. Phys.* **1976**, *64*, 4571.
(58) (a) Funabashi, K. *Adv. Radiat. Chem.* **1974**, *4*, 103. (b) Ichikawa, T.; Yoshida, Y. *J. Chem. Phys.* **1981**, *75*, 5432. (c) McGrane, S. D.; Lipsky, S. *J. Phys. Chem. A* **105**, *2001*, 2384.
(59) Schiff, L. I. *Quantum Mechanics*; McGraw-Hill: New York, 1949; p 76.
(60) Coker, D. F. *J. Chem. Phys.* **1992**, *96*, 652. Coker, D. F.; Berne, B. J. In *Excess Electrons in Dielectric Media*; Ferradini, C., Jay-Gerin, J.-P., Eds.; CRC Press: Boca Raton, FL, 1991; p 211 and references therein. Sheu, S.-Y.; Cukier, R. I. *J. Chem. Phys.* **1991**, *94*, 8258. Space, B.; Coker, D. F.; Liu, Z. H.; Berne, B. J.; Martyna, G. *J. Chem. Phys.* **1992**, *97*, 2002. Chen J.; Miller, B. N. *J. Chem. Phys.* **1994**, *100*, 3013. Chandler, D. *J. Chem. Phys.* **1990**, *93*, 5075 and references therein.
(61) Cubero D.; Quirke, N. *J. Chem. Phys.* **2004**, *120*, 7772. Meunier, M.; Quirke, N. *J. Chem. Phys.* **2000**, *113*, 369.
(62) For example, Abdoul-Carime, H.; Bouteiller, Y.; Desfrançois, C.; Philippe, L.; Schermann, J. P. *Acta Chem. Scand.* **1997**, *51*, 145. Desfrançois, C.; Abdoul-Carmie, H.; Adjouri, C.; Khelifa, N.; Schermann J. P *Europhys. Lett.* **1994**, *26*, 25. These gas-phase anions may be regarded (albeit approximately) as species in which the excess electron interacts as a point charge with a point dipole; the electron orbits this dipole in a diffuse Fermi−Teller orbit. The analogous species in a liquid can also be regarded (albeit approximately) as a point charge at the cavity center interacting with a

point dipole at the cavity wall. The electron wave function is fully confined inside the cavity (i.e., the analogy to the gas-phase dipole-bound anions is incomplete).

(63) Ayotte, P.; Johnson, M. A. *J. Chem. Phys.* **1997**, *106*, 811. Ayotte, P.; Johnson, M. A. *J. Chem. Phys.* **1999**, *110*, 6268. Weber, J. M.; Kim, J.; Woronowicz, E.A.; Weddle, G. H.; Becker, I.; Cheshnovsky, O.; Johnson, M.A. *Chem. Phys. Lett.* **2001**, *339*, 337. Coe, J. V.; Lee, G. H.; Eaton, J. G.; Arnold, S.; Sarkas, H. W.; Bowen, K. H.; Ludewigt, C.; Haberland, H.; Worsnop, D. *J. Chem. Phys.* **1990**, *92*, 3980. Coe, J. V.; Earhart, A. D.; Cohen, M. H.; Hoffman, G. J.; Sarkas, H. W.; Bowen, K. H. *J. Chem. Phys.* **1997**, *107*, 6023.

(64) Verlet, J. R. R.; Bragg, A. E.; Kammrath, A.; Chesnovsky, O.; Neumark, D. M. *Science* **2005**, *307*, 93. Verlet, J. R. R.; Bragg, A. E.; Kammrath, A.; Chesnovsky, O.; Neumark, D. M. *Science* **2004**, *306*, 669. Paik, D. H.; Lee, I.-R.; Yang, D.-S.; Baskin, J. C.; Zewail, A. H. *Science* **2004**, *306*, 672.

(65) Lund, A. *Res. Chem. Intermed.* **1989**, *11*, 37 and references therein.

(66) Gillis, H. A.; Quickenden, T. A. *Can. J. Chem.* **2001**, *79*, 80. Kroh, J. In *Pulse Radiolysis*; Tabata, Y., Ed.; CRC Press: Roca Baton, FL, 1990; p 357 and references therein.

(67) Dye, J. L. *Annu. Rev. Phys. Chem.* **1987**, *38*, 271 and references therein.